Cell

Myelin antigen capture in the CNS by B cells expressing EBV latent membrane protein 1 leads to demyelinating lesion formation

Graphical abstract

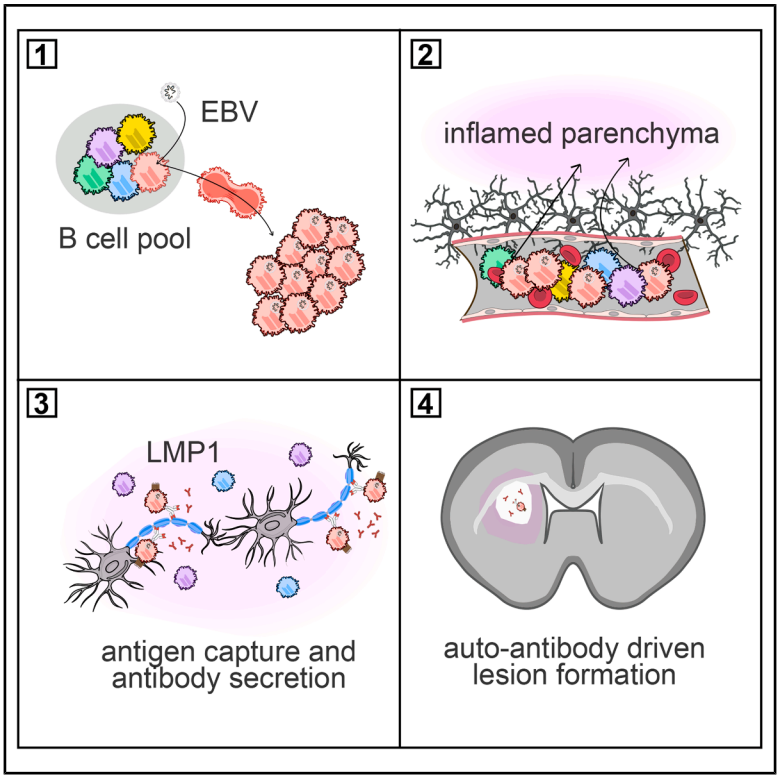

Highlights

- Naive myelin-reactive B cells enter the brain and capture antigen
- B cells capturing antigen in the brain die by activation-induced cell death
- EBV protein LMP1 can rescue B cells from activation-induced cell death
- B cells rescued after antigen capture induce multiple-sclerosis-like demyelinated lesions

Authors

Hyein Kim, Mika Schneider, Yakine Raach, ..., Ludwig Kappos, Nicholas S.R. Sanderson, Tobias Derfuss

Correspondence

nicholas.sanderson@unibas.ch

In brief

Myelin-reactive B cells entering the central nervous system capture cognate antigen from the parenchyma. Without T cell help, they rapidly die; however, Epstein-Barr virus LMP1 enables them to bypass this checkpoint and cause demyelination, as seen in multiple sclerosis.

Kim et al., 2026, Cell *189*, 603–619
January 22, 2026
https://doi.org/10.1016/j.cell.2025.12.031

CellPress

Cell

CellPress
OPEN ACCESS

Article

Myelin antigen capture in the CNS by B cells expressing EBV latent membrane protein 1 leads to demyelinating lesion formation

Hyein Kim,[1,2,8] Mika Schneider,[1,2,8] Yakine Raach,[1,2] Panajotis Karypidis,[1,3] Julien Roux,[1] Georgios Perdikaris,[1,2] Sebastian Holdermann,[1,2] Laila Kulsvehagen,[1,2,3] Anne-Catherine Lecourt,[1,2,3] Kerstin Narr,[1] Roman Sankowski,[4] Martin Diebold,[1,2,3,4] Ewelina Bartoszek-Kandler,[1] Josef P. Kapfhammer,[1] Gert Zimmer,[6,7] Anne-Katrin Pröbstel,[1,2,3] Marco Prinz,[4,5] Ludwig Kappos,[1,2,3] Nicholas S.R. Sanderson,[1,2,9,10,*] and Tobias Derfuss[1,2,3,9]

[1]Department of Biomedicine, University Hospital Basel and University of Basel, Basel, Switzerland
[2]Multiple Sclerosis Centre and Research Center for Clinical Neuroimmunology and Neuroscience (RC2NB), University Hospital Basel and University of Basel, Basel, Switzerland
[3]Department of Neurology, University Hospital Basel, Basel, Switzerland
[4]Institute of Neuropathology, Faculty of Medicine, University of Freiburg, Freiburg, Germany
[5]Signalling Research Centres BIOSS and CIBSS, University of Freiburg, Freiburg, Germany
[6]Institute of Virology and Immunology, Mittelhäusern, Switzerland
[7]Department of Infectious Diseases and Pathobiology, Vetsuisse Faculty, University of Bern, Bern, Switzerland
[8]These authors contributed equally
[9]These authors contributed equally
[10]Lead contact
*Correspondence: nicholas.sanderson@unibas.ch
https://doi.org/10.1016/j.cell.2025.12.031

SUMMARY

The efficacy of B cell depletion therapies, and their association with Epstein-Barr virus (EBV), implicate B cells in the pathogenesis of multiple sclerosis (MS). In mice, we observed that viral infections induce infiltration of B cells into the brain, independent of phenotype and specificity, and that myelin-reactive B cells then capture antigens directly from parenchyma. Trafficking of these antigen-loaded B cells to draining lymph nodes was not observed, and without T cell help, antigen-capturing B cells die rapidly. CD40L signaling or EBV latent membrane protein 1 (LMP1) can override this checkpoint, leading to B cell-receptor- and/or antibody-dependent inflammatory demyelination. Myelin-reactive B cells were identified in the healthy human B cell repertoire, and expression of LMP1 was observed in the brains of a subset of MS patients. These observations can explain the dependency of disease incidence on prior EBV infection, and the increased risk associated with brain infections, and suggest possible treatment strategies.

INTRODUCTION

Multiple sclerosis (MS) is an autoimmune disease of the central nervous system (CNS). Effective treatments either prevent lymphocyte trafficking into the CNS or deplete peripheral B cells, suggesting that CNS infiltration of self-reactive B cells is an important element of the pathomechanism.[1] Lesions in the CNS are characterized by perivascular immune cell infiltration, surrounded by zones of localized destruction of myelin, and one proposed pathomechanism is that a soluble factor released by perivascular immune cells causes the surrounding demyelination.[2] Possible candidates for such a factor, which would explain the dependency of lesion formation on B cells, include autoantibodies[3] or cytokines[4] secreted by B cells themselves,[3] and cytokines from T cells activated by antigens presented by B cells.[4–6]

Either mechanism would require antigen uptake and presentation by myelin-reactive B cells. The model of antibody or cytokine secretion by B cells requires that pathogenic B cells colonize the CNS perivascular space and secrete their products. The antigen-presentation hypothesis needs to explain why B cells have this effect while other professional antigen-presenting cells do not. Particularly for the second problem, the question of where the B cell obtains its antigen is highly relevant. The best-studied location for antigen uptake is the secondary lymphoid organs, where specialized cell types capture and proffer antigens from drained tissues to B cells.[7] B cells are exquisitely sensitive and can stimulate T cells with cognate antigen present at low picomolar concentrations.[8] However, even the abundant CNS proteins neurofilament and glial fibrillary acidic protein (GFAP) are present in the peripheral blood at or below this lower limit,[9] prompting us to investigate

other sources of antigen for B cells. One less well-studied but highly efficient way to acquire antigen is through direct interaction with antigen-expressing cells. B cells have the unique ability to extract their cognate antigen from the membrane of the expressing cell and become activated in the process.[10–13] We hypothesized that naive B cells specific for a CNS-restricted antigen that infiltrated the brain and encountered their cognate antigen might be sufficient to cause demyelination. We observed that B cells died following antigen capture and therefore investigated what additional stimuli are required to rescue them, in particular, whether the only signal lacking is that of T cell help, and whether this can explain the epidemiological finding that infection with Epstein-Barr virus (EBV) appears to be a necessary prerequisite for the development of MS.[14–16]

RESULTS

B cells survey tissues and capture encountered antigen *in situ*

In order to capture antigen directly from infected cells, B cells must enter the tissue. We therefore assessed the abundance of B cells in various organs in healthy wild-type (WT) tomato mice (see STAR Methods). Intravascular cells were labeled by intravenous anti-CD45 antibody injection,[17] and B cells, macrophages, and T cells quantified by flow cytometry (Figures 1A and S1A–S1D). B cells were found in most organs, but in very small numbers in the heart, kidney, and brain, and larger numbers in the lung. Most B cells found in the brain had an immunoglobulin M (IgM)-intermediate, CD19-high, CD20-low phenotype (Figures S1B–S1D), consistent with the interpretation that they are immature B cells characteristically found in the meninges.[18]

To assess the physiological relevance of direct antigen capture, we examined the interaction of influenza A/WSN/33 hemagglutinin (HA)-specific B cells[19] from FluBI mice with influenza-infected cells. First, we examined the kinetics of HA capture *in vitro* by live-cell microscopy (Figure 1B; Video S1).

Following contact, B cells adhere to antigen-expressing target cells. Within 2–10 min of initial contact, antigen can be seen inside the B cell, and by 1 h, some antigen-loaded B cells detach from the target cells. To examine this phenomenon more quantitatively, naive FluBI B cells, or control polyclonal B cells were cocultured with TE-HA-GFP cells and then immunolabeled to assess surface B cell receptor (BCR) and captured HA-GFP. The response was a rapid reduction in surface BCR, in parallel with antigen capture, which continues over 2–4 h (Figures 1C and 1D). To examine antigen capture *in vivo*, we infected mice with influenza A/WSN/33 and, 3 days later, adoptively transferred a mixture of FluBI tomato and WT tomato B cells intravenously and sacrificed mice at 1 or 3 h after transfer. Both types of B cells infiltrated the lungs in equal numbers (Figure 1E) and were found in contact with infected cells (Figures 1F, 1G, and S1E), but FluBI tomato B cells had more intimate contacts with infected cells (Figure 1G; Video S2) at the 1-h time point. These results suggest that antigen capture by naive B cells directly from antigen-expressing parenchymal cells can occur in tissues without involving the lymphoid organs. We next developed a system to study this phenomenon in the CNS.

During infection, virus- and self-reactive B cells enter the brain and capture antigen

In experimental animals, B cells are sparse at steady state but infiltrate the brain following virus infections.[20,21] In humans, CNS infections are a risk factor for MS.[22,23] We studied the kinetics of B cell infiltration into the brains of mice infected intrastriatally with vesicular stomatitis virus (VSV), using two engineered viral preparations. VSV*ΔG is replication incompetent, with the glycoprotein gene replaced by GFP; VSG-G* is weakly replication competent, with a GFP-fused glycoprotein gene, and CNS infection with this virus is fatal for mice within a matter of days. VSV*ΔG readily infected neurons (Figure 2A), but not microglia, astrocytes, or oligodendrocytes (Figure S2A). Infection-induced robust B cell ingress (Figures 2B–2D), initially into the perivascular compartment, but from day 7 onward predominantly into the parenchyma (Figures 2D and S2B).

To track viral antigen capture by B cells in the CNS, we used V10 tomato mice, whose B cells recognize the VSV glycoprotein.[24] We confirmed by live-cell imaging *in vitro* that B cells from this line that contact neurons infected with VSV-G* arrest and extract antigen from the infected cell membrane (Figures 2E and 2F; Video S3).

To follow the same interaction *in vivo*, we infected V10 tomato mice in the striatum with VSV*ΔG to induce B cell infiltration, then 5 days later reinfected them in the superficial cortex with VSV-G*, mediating expression of the VSV glycoprotein. 2 days later, we visualized the interaction between B cells and VSV-G*-infected cells by two-photon microscopy (Figure 2G; Video S4). As seen *in vitro*, B cells arrested on infected cells after contact and appeared to capture antigen. To quantitatively confirm antigen capture and presentation, we infected V10 tomato mice with VSV*ΔG intrastriatally, reinfected them with VSV-G* 7 days later, and retrieved B cells from the brain and lymphoid organs 2 days thereafter for coculture ELISpot assays with VSV glycoprotein-specific L7 T cells.[25] Antigen was presented only by B cells retrieved from the brain, not by B cells from draining lymph nodes or elsewhere (Figure 2H). Sensitivity and specificity of the ELISpot assay were confirmed with positive and negative controls (Figure S2C).

Having established the parameters of tissue antigen capture by B cells in a viral paradigm, we next developed a system to investigate the phenomenon in the context of autoimmunity. We used mice whose B cells recognize the CNS-restricted myelin oligodendrocyte glycoprotein (MOG)[26] and express tdTomato (MOG tomato mice). Antigen capture by these B cells resulted in transcriptional changes similar to those induced by BCR stimulation with anti-IgM antibodies (Figure S2D). We confirmed by two-photon microscopy that they extravasate into the virus-infected brain, but not under non-inflamed conditions (Figure 2I; Videos S5 and S6). We then repeated the intrastriatal infection paradigm in MOG tomato and WT tomato mice, retrieved brain-infiltrating B cells 7 days after infection, and interrogated them by interferon-γ ELISpot with MOG-specific 2D2 T cells. As in the viral paradigm, antigen-presenting B cells were retrieved only from the brain, not from draining lymph nodes or elsewhere (Figures 2J, S2C, and S2E). Antigen-irrelevant B cells from WT tomato mice were unable to capture and present antigen, regardless of their anatomical origin.

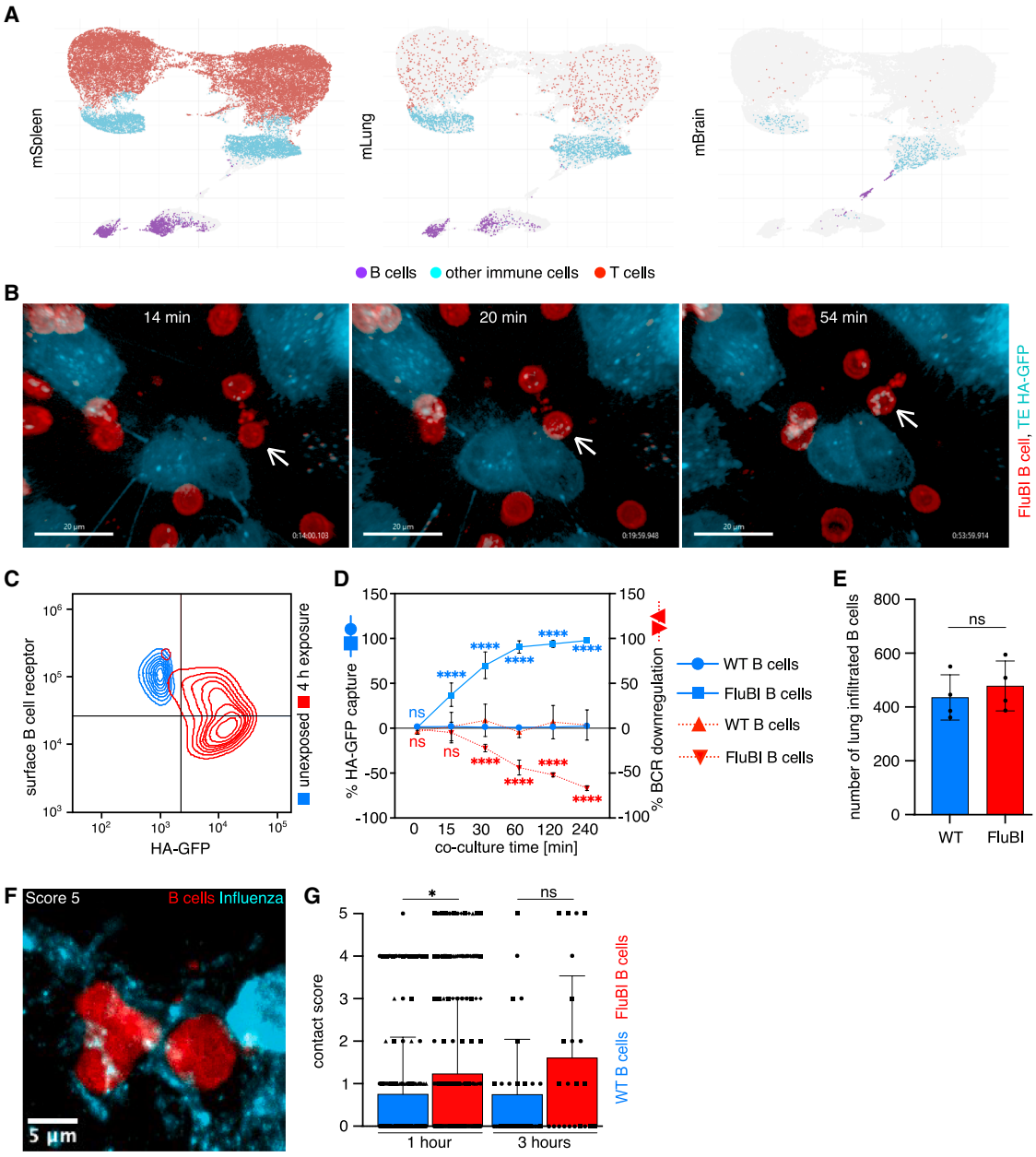

Figure 1. Antigen surveillance by B cells

(A) Tissue-infiltrating immune cells in various mouse tissues. Each figure is an omnibus uniform manifold approximation and projection (UMAP) of 50,000 cells in total in light gray, with a superimposition of cells from the specified organ, colored according to cluster. See also Figures S1A–S1D.

(B) Influenza hemagglutinin (HA) capture by FluBI B cells *in vitro*—live-cell microscopy. The white arrow shows a B cell (red) before contact in the first frame, then immediately after contact with an HA-GFP-expressing cell (cyan) in the second frame, and following antigen capture and detachment in the last frame. Scale bar, 20 µm. See also Video S1.

(C and D) HA capture by FluBI B cells *in vitro*—flow cytometry. FluBI or polyclonal B cells were cocultured for various lengths of time with TE-HA-GFP cells. (C) Surface BCR and captured HA-GFP in FluBI B cells at baseline (blue contours) and after 4 h (red contours). (D) Time course of HA capture. Left vertical axis: HA-GFP as a percentage of maximum (blue); right vertical axis: percentage loss of surface BCR (red). Horizontal axis: duration of coculture. $n = 9$. ****$p < 0.0001$ two-way ANOVA, Sidak's multiple-comparisons test.

(E) Lung infiltration by WT or FluBI B cells during infection. Unpaired, two-tailed *t* test.

(F and G) Interaction between B cells and infected cells in lung. FluBI tomato or WT tomato B cells were transferred into infected C57BL/6 mice. (F) Confocal micrograph of FluBI cells (red) interacting with infected lung cells (cyan). Scale bar, 5 µm. See also Video S2. (G) Characterization of contacts between B cells and infected cells. Typical images for each score are shown in Figure S1E. *$p = 0.0132$, two-way ANOVA with time point and B cell specificity as factors, followed by Sidak's multiple-comparisons test. All bars indicate means; error bars indicate standard deviation.

See also Figure S1.

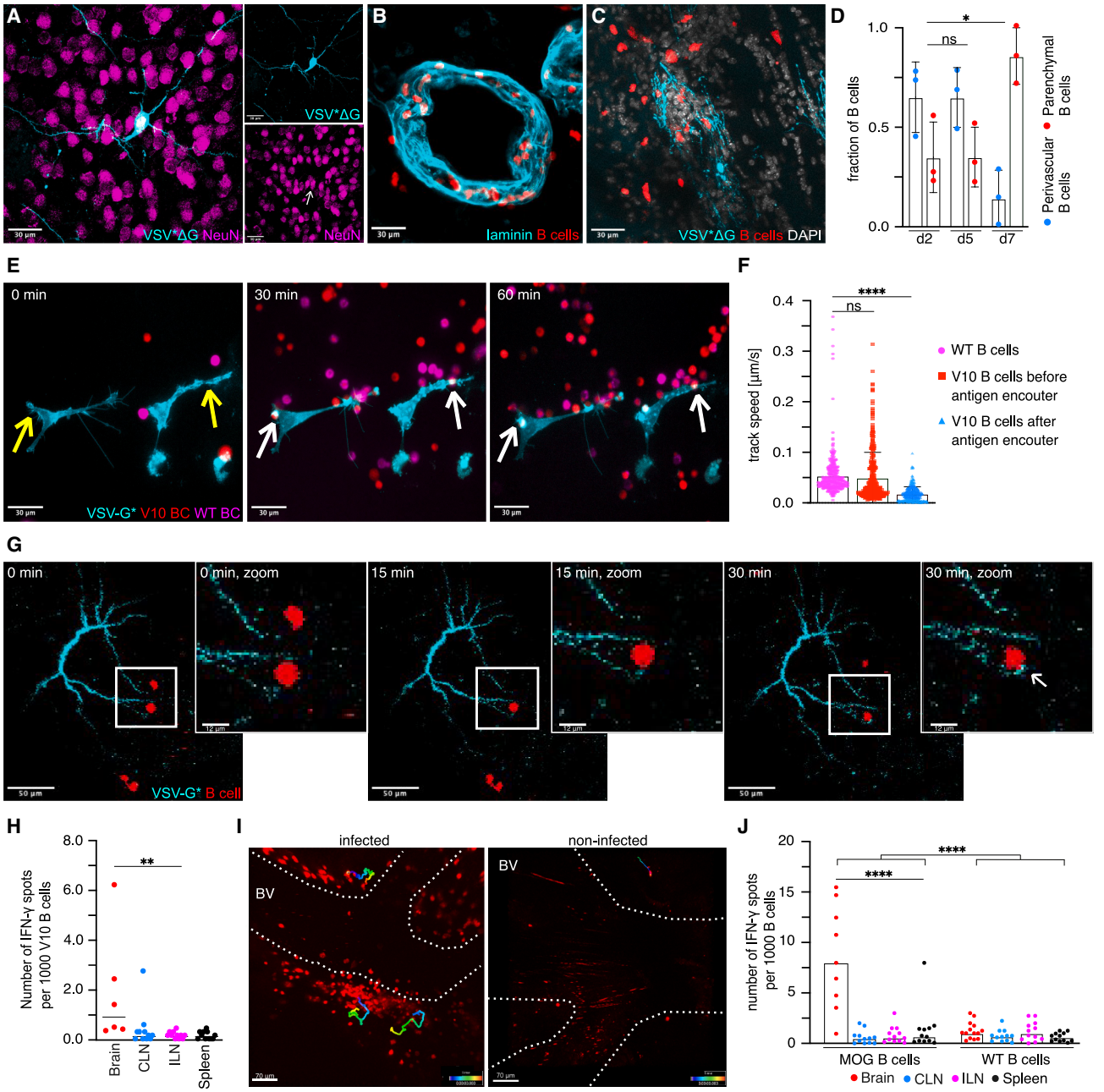

Figure 2. Brain infiltration and antigen capture by B cells

(A) Infection of neurons (NeuN, magenta) by VSV*ΔG (GFP, cyan). Scale bar, 30 μm.

(B–D) Infiltration of B cells (red) into the brain following VSV*ΔG infection. (B) Perivascular B cells. Laminin immunolabeling (cyan) indicates the vascular basement membrane. (C) Parenchyma-infiltrating B cells (red) in the vicinity of an infected cell arbor (GFP, cyan). DAPI in white. (D) B cell infiltration kinetics. *p = 0.0132, one-way ANOVA, Dunnett's multiple-comparisons test.

(B and C) Scale bar, 30 μm. See Figure S2B.

(E) Live-cell microscopy of antigen capture by V10 tomato B cells from mouse primary cerebral cortical cells infected with VSV-G*. Yellow arrows in the left-most image show points of subsequent contact by B cells; white arrows show B cells acquiring antigen at the same loci at later time points. Scale bar, 30 μm. See also Video S3.

(F) Velocities of B cells during antigen capture. (****$p < 0.0001$ one-way ANOVA followed by Dunn's multiple-comparisons test).

(G) Intravital imaging of antigen capture by V10 tomato B cells (red) in the cerebral cortex. GFP expressed by infected cells is shown in cyan. Main panels show the infected cell and several infiltrating B cells (scale bar, 50 μm). Insets show zoomed images of contacts between the infected cell and B cells. White arrow in the right-most image indicates the zone of antigen capture. Scale bar, 12 μm. See also Video S4.

(legend continued on next page)

Combined with the results from the lung, the capture of antigen in the brain makes it clear that B cells can capture antigen in non-lymphoid tissues directly from antigen-expressing cells.

Antigen encounter by naive B cells leads to deletion

We hypothesized that MOG-reactive B cells infiltrating the brain and activated by membrane antigen capture would cause localized demyelination. We therefore examined myelin integrity by histology at various time points after intrastriatal infection, but at no point did we observe any demyelination (Figure S3A). We quantified infiltrating B cells at each time point and observed that, compared with WT tomato B cells, MOG tomato B cells were significantly fewer (Figure S3B), suggesting that antigen-encountering B cells were specifically eliminated. To investigate this possibility, we repeated the infection paradigm with MOG tomato and WT tomato mice, sacrificed them at 7 or 21 days post-infection, and quantified the numbers of MOG-reactive (IgM^a+) B cells by flow cytometry. At both time points, around 90 % of peripheral B cells but fewer than 20 % of brain-infiltrating B cells were IgM^a+ (Figure 3A). These results are consistent with the hypothesis that autoantigen-encountering B cells are rapidly eliminated by activation-induced cell death (AICD).[27] This predicts that at early time points after brain infiltration, autoreactive cells will be recently activated and, at later time points, absent, whereas non-reactive B cells should be non-activated and, counterintuitively, survive longer. We tested these predictions by intrastriatally infecting MOG tomato and FluBI tomato mice, sacrificing them 7 or 21 days later, and comparing the transcriptomes of brain-infiltrating B cells by single-cell RNA sequencing (scRNA-seq) (Figures 3B–3F), enabling us to assign each cell unequivocally to the MOG-reactive or HA-reactive pools, or as non-transgenic bystander B cells (Figures 3C and 3D). Overall numbers of infiltrating B cells were higher in the FluBI tomato mice compared with the MOG tomato group (Figures 3C and 3D). Most B cells in the brains of MOG tomato mice were non-transgenic, and the *bona fide* MOG transgenic B cells were largely eliminated. At day 7 after infection, two substantial populations of MOG tomato transgenic B cells remained in the brains: one population of cells with a pre-B or transitional phenotype, marked with a yellow ellipse in Figure 3C, that are likely to be meningeal,[18] and one population identified as GC-like, (magenta ellipse in Figures 3C, 3E, and 3F). Of these two populations, the immature, putatively meningeal population was still present at day 21, consistent with a non-parenchyma location and non-exposure to antigen. The second population of GC-like cells (cluster 1 on Figure 3B) was almost completely eliminated by day 21, and we focused on this cell population as likely to include MOG-reactive, mature B cells interacting with antigen in the parenchyma.

To assess the role of AICD, cells were plotted according to their expression of genes controlled by the transcription factor TFEB, a central regulator of AICD after antigen exposure.[28] Among MOG-specific B cells, high expression of TFEB-regulated genes was mostly restricted to the GC-like population (Figure 3E). Not surprisingly, very few of the antigen-irrelevant FluBI transgenic B cells were seen in the TFEB-signature-high, GC-like population. These results are consistent with the hypothesis that naive B cells that encounter their cognate antigen in the brain die by AICD. At day 7, this population of B cells also exhibited a signature of recent antigen capture derived from the bulk sequencing experiment shown in Figure S2D (Figure 3F), and this signature was largely absent by day 21.

Death by AICD occurs when B cells encounter antigen but lack T cell help.[27] We examined this *in vitro* by exposing MOG-specific B cells to MOG-expressing cells and then coculturing them with 2D2 T cells. B cells exposed to both antigen and cognate, naive T cells proliferated robustly, but not under any other condition (Figure 3G).

Myelin antigen capture by B cells in brain does not stimulate a T cell response *in vivo*

The above results suggest that if brain-infiltrating, MOG-reactive B cells could obtain T cell help, they would proliferate. We repeated the experiment inducing lymphocyte infiltration with intrastriatal VSV*ΔG infection in MOG tomato mice, but with the addition of adoptive transfer of 30 million MOG-specific 2D2 T cells or non-transgenic control T cells. In this paradigm, antigen presentation by MOG-presenting B cells ought to lead to widespread activation of these highly encephalitogenic T cells, detectable by the motor signs of experimental autoimmune encephalomyelitis (EAE) and inflammatory lesions in the CNS; however, this was not observed. At sacrifice, 28 days post-infection, both B cells and T cells could be seen infiltrating the brains of these mice, but surrounding myelin was intact (Figure 3H), motor behavior was normal for both groups, and their weights were stable (Figure 3I). We quantified the brain-infiltrating B cells to assess B cell proliferation; however, the results instead suggested that MOG-specific B cells were, if anything, fewer than WT B cells (Figure 3J). We also tested the reversed paradigm, with B cell transfer into T cell receptor (TCR) transgenic mice, but obtained similar results (Figure S3C). These results suggest that naive T cells are unable to rescue recently antigen-capturing B cells from AICD, although this may reflect inadequate expression of chemokine receptors or other molecules required for brain ingress.[29] We therefore compared the impact of

(H) Antigen presentation by brain-infiltrating, virus-specific B cells assessed by interferon-γ ELISpot. Data pooled from three experiments. $^{**}p < 0.0013$, one-way ANOVA followed by Dunnett's multiple-comparisons test.

(I) Intravital microscopy of brain-infiltrating, myelin-reactive B cells. Left: MOG tomato B cells (red) infiltrating the infected cortex from a blood vessel (white outlines). Colored lines show tracks of three parenchyma-infiltrating B cells (rainbow colors: blue = time 0, red = time 50 min). Right: a similar image from non-VSV-infected mouse. Scale bars, 70 μm. Full sequences are shown in Videos S5 and S6.

(J) Antigen presentation by brain-infiltrating, myelin-specific B cells assessed by interferon-γ ELISpot. Vertical axis: number of interferon-γ spots per 1,000 B cells. Each point corresponds to result from one mouse or, in one experiment, pooled cells from four mice. Data were combined from three experiments. $^{****}p < 0.0001$ two-way ANOVA with a significant interaction, followed by Sidak's multiple-comparisons test. All bars indicate means; error bars indicate standard deviation. See also Figure S2.

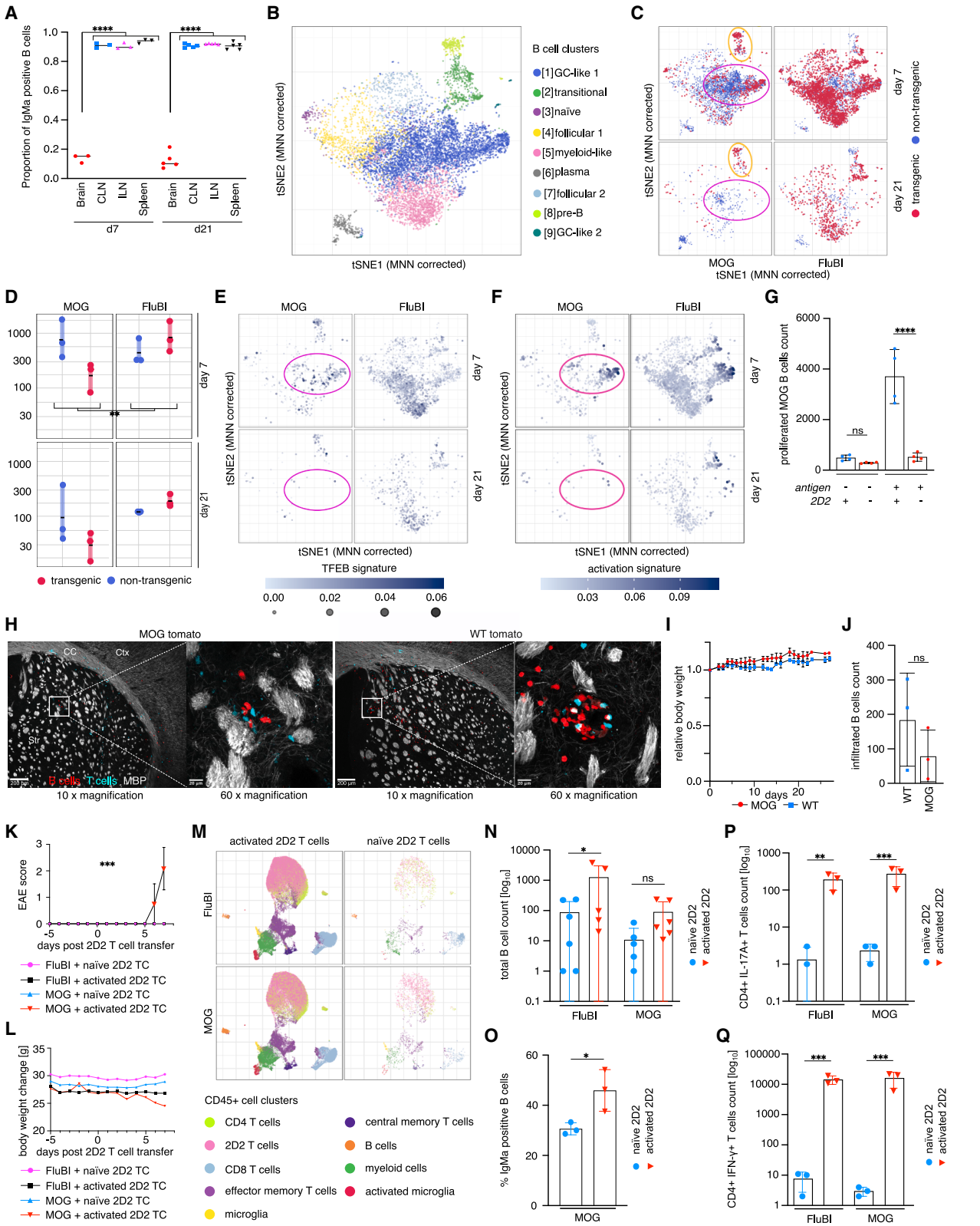

(legend on next page)

transferring naive or *ex vivo*-activated 2D2 T cells into mice with MOG-reactive or HA-reactive B cells. Transfer of activated 2D2 T cells led to motor signs typical of EAE in some animals (Figure 3K) as well as weight loss (Figure 3L). All mice were sacrificed as soon as any mice reached a score of 3 (all such cases occurred in the condition with MOG-reactive B cells + activated 2D2 T cells). Immune cells were retrieved from the brains for flow cytometry (Figures 3M–3Q and S3D–S3L) to determine whether activated T cells had been able to rescue the B cells. Transfer of activated 2D2 T cells led to greater abundance of immune cells in the brain, including B cells (Figure 3N). The number of MOG-reactive B cells as a fraction of total B cells in the brain was increased by activated 2D2 T cells (Figure 3O), consistent with antigen-specific rescue. Production of interferon-γ, interleukin (IL)-17, IL-2, and IL-10 cytokines by brain-infiltrating T cells (Figures 3P, 3Q, S3G, and S3H), activation and proliferation of T cells as shown by CD69 and KI67 expression (Figures S3E and S3F), and activation of microglia as shown by Clec7a and P2RY12 expression (Figure S3L) were observed only in the activated 2D2 condition; however, there was no evidence that these were influenced by interactions with cognate B cells. To confirm that the lack of a productive interaction between MOG-capturing B cells and naive 2D2 T cells was not due to absence of the requisite signaling molecules, we also measured and confirmed robust expression of CD40 and major histocompatibility complex class II (MHC class II) on the majority of brain-infiltrating B cells (Figures S3I–S3K).

B cells that recognize antigen in the brain can be rescued by CD40L signaling

The most important signal provided by T cells to rescue antigen-exposed B cells from AICD is CD40L,[30] and we investigated whether this was the missing signal for brain-infiltrating, myelin-reactive B cells. We first modeled the phenomenon *in vitro*, using MOG tomato B cells exposed to antigen and then provided T cell help or CD40L stimulation. As expected, B cells exposed to antigen and cultured alone died within 6 days, as did antigen-non-exposed B cells (Figure 4A). Coculture with cognate T cells enabled proliferation and survival of B cells, conditional on the B cells having captured antigen, and CD40L stimulation mimicked this effect independently of antigen. To investigate the same phenomenon *in vivo*, we repeated the paradigm of intrastriatal VSV*ΔG infection, but in some mice induced intrastriatal expression of CD40L by adenoviral vector administration. Histology confirmed that MOG-reactive B cells were rescued by CD40 signaling in this context: B cell numbers in the brain were roughly tripled compared with MOG tomato mice without CD40L expression (Figures 4B and 4C). In MOG tomato mice with CD40L rescue, localized areas of demyelination together with IgM deposits were observed around the B cell infiltrates (Figures 4D and 4E).

To study the phenotypes of the rescued B cells, we repeated the experiment and subjected brain-infiltrating B cells to scRNA-seq, and compared their transcriptomes between groups (Figures 4F and S4B). More B cells were observed overall in the brains of MOG tomato mice when exogenous CD40L was provided, including both transgenic and bystander B cells. However, one subpopulation of B cells among the MOG-specific transgenic B cells was specifically spared by CD40L, namely the germinal center-like B cells (Figures 4G and 4H), These cells were associated with recent antigen capture and with the AICD fate in the first scRNA-seq experiment (Figures 3B–3F) and were completely depleted in the absence of CD40L (Figures 4G and 4H). These results are consistent with the hypothesis that antigen-encountering B cells in the brain are normally deleted by AICD due of the absence of CD40 signaling following BCR stimulation. CD40 and MHC class II were abundantly expressed on most brain-infiltrating B cells (Figure 4I).

B cell expression of the EBV protein LMP1 circumvents the CD40L checkpoint

Because naive T cells were unable to rescue brain-infiltrating myelin-reactive B cells from AICD (Figure 3), B cell antigen capture in the CNS followed by antigen presentation to T cells

Figure 3. Fate of brain-infiltrating MOG-reactive B cells

(A) Proportions of MOG-reactive B cells in brain and periphery at days 7 and 21. ****$p < 0.0001$, two-way ANOVA, followed by Dunnett's multiple-comparison tests, non-significant interaction term and no significant effect of time point.

(B–F) scRNA-seq data from B cells infiltrating the mouse brain. (B) Omnibus t-SNE plot of B cells. Gene expression levels defining the clusters shown in the heatmap in Figure S4A. (C) t-SNE plot as in (B), but colored for each condition as expressing transgenic (red) or non-transgenic "bystander" (blue) immunoglobulin genes. The yellow ellipse delineates a population of immature, putatively meningeal B cells. The magenta ellipse delineates a population of germinal center (GC)-like B cells that are eliminated among the MOG-specific B cells by day 21 after infection. (D) Numbers of B cells assigned in each condition to transgenic (MOG or FluBI) or non-transgenic at the two time points (7 and 21 days after infection). **False discovery rate (FDR) = 0.0037. (E) t-SNE plot as in (B), restricted to transgenic B cells (either MOG or FluBI) and colored according to expression of a panel of TFEB-related genes.[28] (F) Similar t-SNE plot colored according to expression of a panel of antigen-capture-induced genes extracted from the experiment shown in Figure S1F.

(G) Influence of T cell help on B cell proliferation after antigen capture *in vitro*. ****$p < 0.0001$, two-way ANOVA followed by Dunnett's multiple-comparisons test. Results pooled from two experiments.

(H–J) Influence of naive cognate T cells on the outcome of B cell brain infiltration over 28 days after intrastriatal VSV*ΔG infection. (H) Confocal micrographs of striatum-infiltrating B and T cells at day 28. White indicates immunolabeling for MBP (myelin basic protein). tdTomato (B cells) in red and 2D2 T cells in cyan. Scale bars, 20 or 200 μm. Ctx, cerebral cortex; CC, corpus callosum; Str, striatum. (I) Weights of mice compared with baseline over 28 days of observation. (J) Numbers of brain-infiltrating B cells in MOG tomato and WT tomato mice at day 28. ns: $p = 0.3032$ unpaired, two-tailed *t* test.

(K–Q) Influence of activated cognate T cells on the outcome of B cell brain infiltration.

(K) Clinical scores over time. ***$p = 0.0006$, Fisher's exact test. (L) Weights of mice over time. (M) UMAP plots of $CD45^+$ cells retrieved from brains of mice shown in (K). (N) Numbers of B cells in brains. *$p = 0.0245$. (O) Numbers of MOG-reactive B cells as percentage of total B cells. *$p = 0.03775$, two-tailed *t* test. (P) Numbers of 2D2 T cells from brains positive for IL-17. **$p = 0.0095$. (Q) Analogous figure for interferon-γ. ***$p < 0.001$. All bars indicate means; error bars indicate standard deviation.

See also Figures S3 and S4.

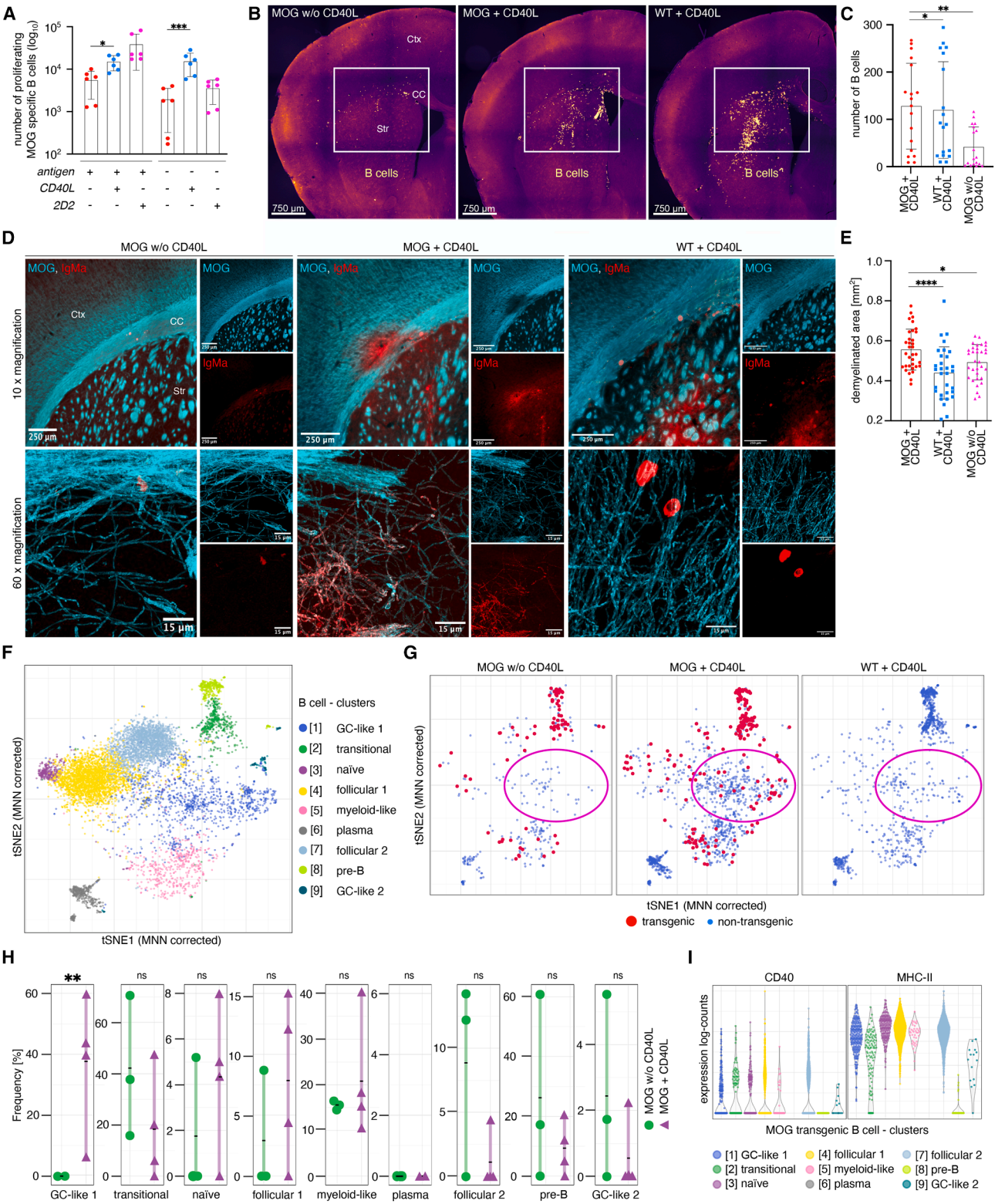

Figure 4. B cell rescue by CD40L following antigen capture

(A) Antigen-capturing B cell rescue by CD40L in the absence of T cells *in vitro*. *p = 0.0148, ***p = 0.0009, two-way ANOVA with a non-significant interaction, followed by Sidak's test.

(legend continued on next page)

in situ cannot be the initiating trigger in the formation of lesions. Activated T cells can rescue B cells after antigen capture (Figure 3), but this would require T cell priming in the periphery. We therefore considered alternative sources of the CD40L survival signal other than T cells.

One candidate is EBV. Strong epidemiological evidence suggests that EBV infection is a necessary prerequisite for the development of MS,[16] and the rescue of naive B cells into the memory compartment is fundamental to the virus' lifecycle.[31] In particular, the viral latent membrane protein 1 (LMP1) functions as a constitutively active CD40 mimic.[32] LMP1 is only expressed in a subset of viral latency programs but is induced by BCR stimulation.[33] To study the influence of LMP1 expression on the fate of antigen-capturing B cells experimentally, we generated mouse lines in which tamoxifen treatment induced the expression of tomato alone (MOG tam(tomato)) or tomato and LMP1 (MOG tam(LMP1 tomato)) in MOG-specific B cells, or in polyclonal B cells (WT tam(LMP1 tomato)) (Figures 5A and S5A, see also STAR Methods). We repeated the *in vitro* antigen-exposure survival experiment but replaced CD40L stimulation with tamoxifen-induced LMP1 expression in B cells. Similar to CD40L stimulation, LMP1 expression facilitated B cell survival; however, unexpectedly, proliferation was significantly higher in B cells that both expressed LMP1 and encountered antigen than in those cells that expressed LMP1 but remained antigen-naive (Figure 5B). This synergistic interaction between BCR stimulation and LMP1 signaling offers a good mechanistic explanation for the formation of localized demyelinating lesions caused by CNS-infiltrating, autoreactive B cells. We compared the transcriptional impact of LMP1 expression versus CD40L signaling at 4 (Figure S5B) or 24 h (Figure 5C) after antigen capture and found that the impact of the two signals was quite similar, with only one gene (Tmem123) significantly differentially regulated between the two conditions (Figure 5C).

To examine the impact of LMP1 expression during antigen capture in tissue, we studied the interaction of these B cells with myelin *ex vivo* using cerebellar slice cultures. MOG tam(LMP1 tomato), but not WT tam(LMP1 tomato), B cells induced extensive demyelination within 1 week (Figures 5D–5F). To investigate the mechanism of demyelination, we labeled these slices for the microglial marker Iba1 and observed dense clusters of Iba1-expressing cells at foci of demyelination. To clarify whether the activity of these microglial cells was a cause or a result of the demyelination process, we depleted slice cultures with PLX5622 (Figure 5G). Increasing doses of the drug resulted in sparser Iba1 labeling but more intact myelin. To quantify this phenomenon, we switched to a more microglia-specific genetic system using Csf1r$^{fl/fl}$ mice crossed with Cx3cr1-CreERT2-eYFP, in which tamoxifen mediates the depletion of microglia. In this paradigm as well, microglial depletion reduced the demyelination otherwise induced by LMP1-expressing MOG-reactive B cells (Figure 5H).

Brain infiltration of LMP1-expressing, MOG-reactive B cells leads to demyelination *in vivo*

To examine the impact of LMP1 expression on autoreactive B cells *in vivo*, we injected animals intrastriatally with VSV*ΔG, 2 days later with B cells from tamoxifen-treated littermates, and 12 days later sacrificed them for histology (Figures 6A–6E). A simpler paradigm of treating the animals systemically with tamoxifen was not possible because global expression of LMP1 in B cells leads to fatal splenomegaly (Figures S5C and S5D). In mice given WT tam(LMP1 tomato) or MOG tam(LMP1 tomato) B cells, more B cells were observed in the brain than in mice given MOG tam(tomato) B cells (Figure 6B). However, only in the MOG tam(LMP1 tomato) mice, the surrounding tissue was strikingly demyelinated (Figures 6A, 6C, and S5E). To investigate possible effector mechanisms involved in the demyelination, we examined deposition of complement components C1q and C3d (Figures 6D, 6E, S5F, and S5G). C1q was significantly more abundant around the lesions in MOG tam(LMP1 tomato) than in MOG tam(tomato) mice, and C3d was increased both in this group and in the WT tam(LMP1 tomato) group.

Finally, we considered the possibility that B cells rescued by LMP1 might survive long enough to present antigen to T cells. To test this, we transferred MOG tam(tomato) or MOG tam(LMP1 tomato) into 2D2 mice (F1 hybrids of BALB/c mice with 2D2 on a C57BL/6 background, to avoid allogeneic rejection). We were not expecting a dramatic motor phenotype from lesions in the forebrain, but we monitored them over time using a limb-use asymmetry test[34] to detect unilateral motor deficits. At 16 and 21 days after virus infection, we sacrificed cohorts of mice and quantified and phenotyped brain-infiltrating immune cells by flow cytometry. Preferential use of the limb ipsilateral to the injection site (Figure 6F) was not seen in the MOG tam(tomato) group and peaked in the MOG tam(LMP1 tomato) group with WT T cells at 12 days, and in the MOG tam(LMP1 tomato) group with 2D2 T cells at 16 days after infection, but neither of these reached statistical significance ($p = 0.069$). At the sacrifice time points, the presence of MOG tam(LMP1 tomato) B cells led to

(B–E) Brain-infiltrating, MOG-reactive B cells are rescued by CD40L and initiate demyelinating lesions. Six mice per condition, pooled from two experiments. (B) Fluorescence microscopy of striatum-infiltrating B cells. Scale bar, 750 μm. Yellow indicates tdTomato (B cells). Ctx, cerebral cortex; CC, corpus callosum; Str, striatum. White boxes delineate areas of infection and B cell infiltration. (C) Quantification of infiltrating B cells in images as in (B). Each point represents the mean count of infiltrating B cells across 5 or 6 sections from one mouse. *$p = 0.0123$, **$p = 0.0055$, one-way ANOVA, followed by Dunnett's test. (D) Myelin visualized by immunofluorescence microscopy. Upper: 10× images of similar sections to those shown in (B). Scale bar, 250 μm. Immunolabeling for myelin (cyan), and IgM^a (red). Lower: 60× confocal images showing myelinated fibers of the dorsal striatum undergoing demyelination. Scale bars, 15 μm. Ctx, cerebral cortex; CC, corpus callosum; Str, striatum. (E) Quantification of demyelinated areas shown in coronal sections through the striatum. Each point represents the mean demyelinated area in one section. *$p = 0.0470$, ****$p < 0.0001$ one-way ANOVA followed by Tukey's test.

(F–I) scRNA-seq data from brain-infiltrating B cells rescued by CD40L. (F) t-SNE plot of B cells retrieved from mouse brains with or without CD40L. Genes characterizing the clusters are shown in Figure S4B. (G) t-SNE plots as in (F), split by condition and colored by transgenic assignment. The magenta ellipse shows the GC-like population identified in Figures 3B–3F. (H) Frequencies of MOG transgenic B cells assigned to each cluster, with or without CD40L rescue. **FDR = 0.0024. (I) CD40 and MHC expression on B cells in each cluster. All bars indicate means; error bars indicate standard deviation.

See also Figure S4.

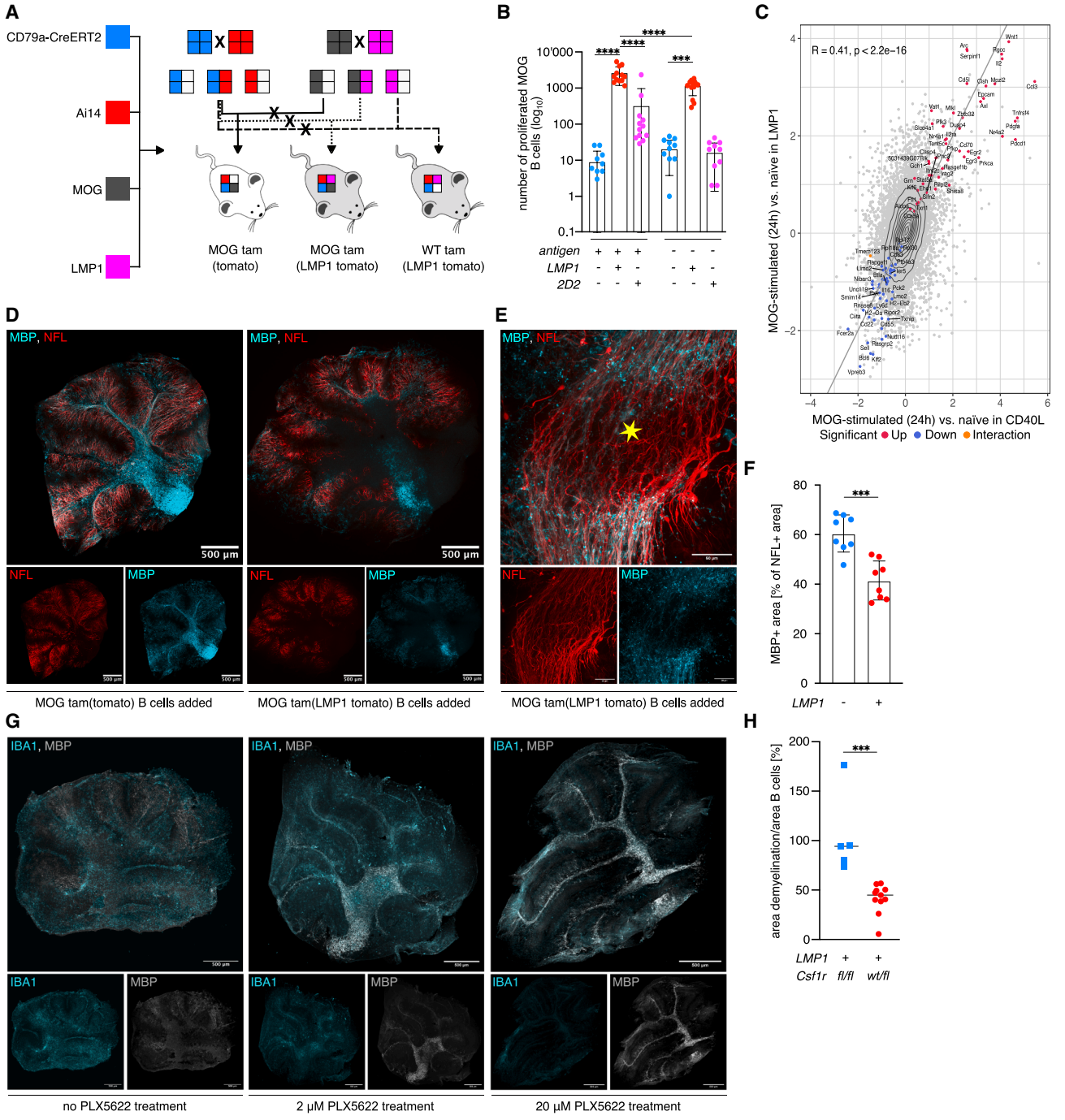

Figure 5. B cell expression of LMP1 replaces the CD40L signal

(A) Mouse breeding scheme. Genotypes shown on the left (see STAR Methods) are represented as colored squares in the pedigree tree on the right. Offspring from these crosses were used for experiments in this figure and Figure 6. See also Figure S5A.

(B) Influence of LMP1 expression on B cell proliferation after antigen capture *in vitro*. Each point shows results from one coculture well. Data are pooled from three experiments. ***$p = 0.0003$, ****$p < 0.0001$, two-way ANOVA followed by Tukey's test.

(C) Comparison of gene expression following antigen capture between B cells expressing LMP1 and exposed to CD40L signaling.

(D–F) Demyelination induced by MOG tam(LMP1 tomato) B cells in cerebellar slice cultures. Scale bar: 500 µm in (D) and 50 µm in (E). (F) Quantification of demyelination. ***$p = 0.0002$, unpaired, two-tailed *t* test.

(G) Depletion of microglia and rescue of myelin by PLX5622. Scale bar, 500 µm.

(H) Quantification of demyelination induced by MOG tam(LMP1 tomato) B cells with ($Csf1r^{fl/wt}$) or without ($Csf1r^{fl/fl}$) microglia depletion. ***$p = 0.0005$, unpaired, two-tailed *t* test. All bars indicate means; error bars indicate standard deviation.

See also Figure S5.

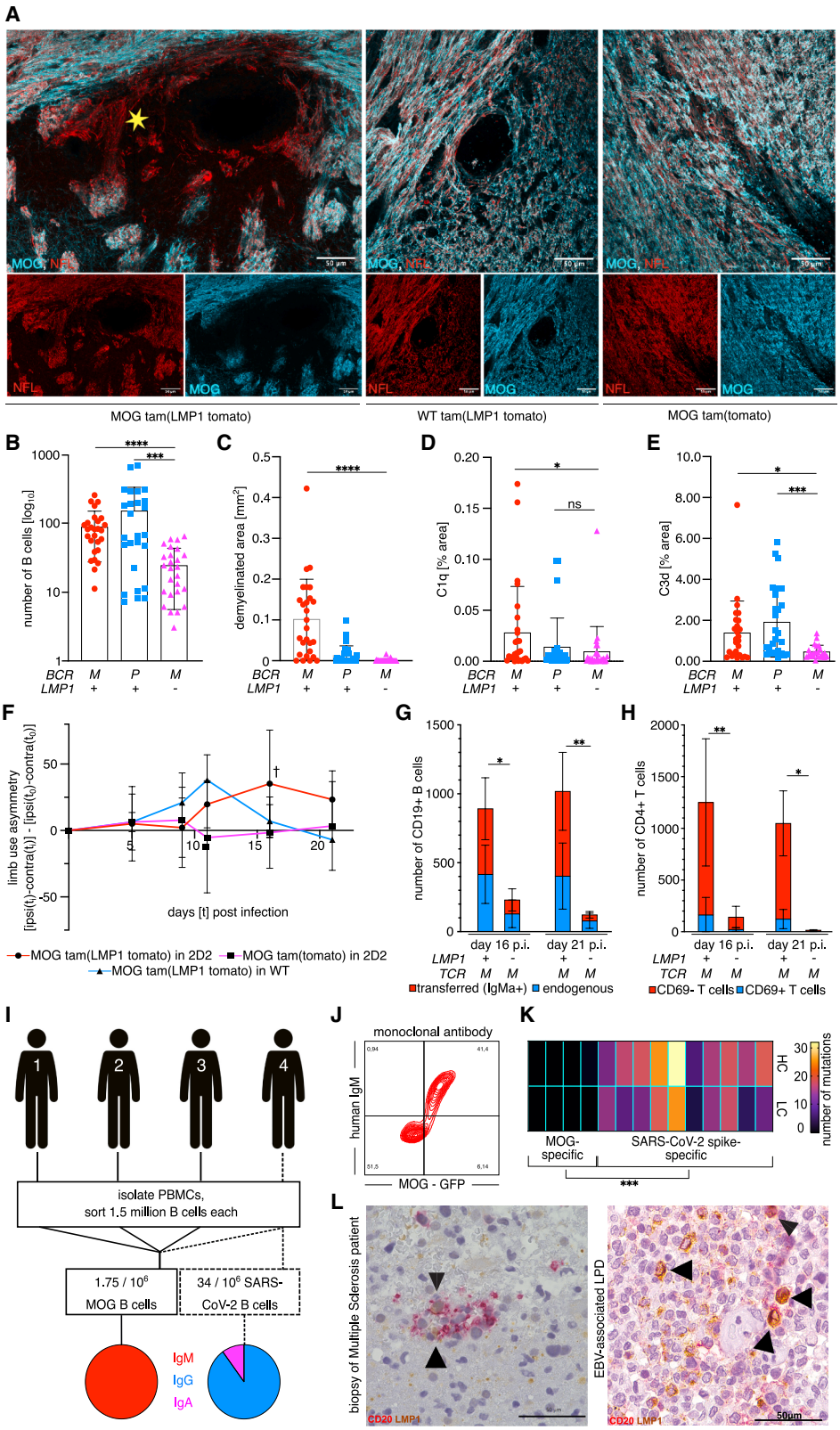

(legend on next page)

significantly greater number of B cells (Figure 6G), as expected, but also significantly greater infiltration and activation of T cells (Figure 6H) than the MOG tam(tomato) B cells. The majority of infiltrating T cells had a memory phenotype ($CD44^+$, $CD62L^-$) (Figure S5H).

Relevant components of the proposed model are observed in humans

To examine the plausibility of an etiological model based on direct antigen capture by myelin-reactive B cells within the CNS in humans, we assessed the frequency of B cells with this capability. We screened unfractionated blood B cells from four healthy donors by membrane antigen capture-activated cell sorting (MACACS)[35,36] (Figure 6I; Table S1). MACACS-positive cells were expanded, and the binding of their secreted antibodies checked for MOG specificity (Figure S5I). We expressed one of the identified human IgM antibodies against MOG and verified its binding in a live cell-based assay (Figure 6J). For one donor, we performed the same steps in parallel using the SARS-CoV-2 spike protein as a model antigen against which the donor had mounted a physiological immune response. The average frequency of MOG-specific B cells was 1.75 per million (0.3, 0.8, 2.6, and 3.3), and that of spike-specific B cells was 34 per million B cells. All MOG-specific B cells expressed IgM, whereas all of the spike-specific B cells were either IgG or IgA (Figure 6I). The immunoglobulin genes of MOG-specific B cells were all germline, whereas those of spike-specific B cells showed varying degrees of somatic hypermutation (Figure 6K), suggesting that the autoreactive population is restricted to the naive compartment.

Another requirement of a model involving brain infiltration by autoreactive, LMP1-expressing cells is that such cells ought to be detectable in MS lesions. Expression of LMP1 in brain-infiltrating B cells has been reported,[37–39] but is controversial.[40] We examined biopsy or autopsy samples from the brains of six donors with MS and six controls (Table S1) and found, in lesions from two donors, a small number of cells that labeled positively for CD20 and LMP1, similar to those found in tissue from a donor with a lymphoproliferative disorder, in which such cells were numerous (Figures 6L, S5J, and S5K).

DISCUSSION

A model of the pathogenesis of MS must explain the strong association with EBV infection and the therapeutic efficacy of B cell depletion. MS relapses are largely eliminated by peripheral B cell depletion before global antibody levels change, suggesting that relapses must be caused by a *de novo* action of CD20 B cells rather than by antibodies accumulated over time. We show (1) that in animal models naive, myelin-reactive B cells enter the CNS during infections, (2) that they can capture antigen directly from previously healthy myelin, and (3) that the EBV protein LMP1 can rescue them from the normal tolerance mechanism of AICD. In mice, this leads to the formation of demyelinated lesions surrounding perivascular accumulations of immune cells, very reminiscent of CNS lesions seen in patients with MS. These findings support a model of MS pathogenesis in which a myelin-reactive B cell is infected with EBV in adolescence and expands into a clone of memory-like cells. It is known from epidemiological studies that a CNS infection between the ages of 11 and 19 years increases the risk to later develop MS nearly 3-fold, whereas brain infections at a younger age or infections in other organs are less predictive.[22,23] Previous head trauma also increases the risk.[41] These events have in common that they involve temporary disruption of the blood-brain barrier and elevated immune cell infiltration. During a CNS infection, some of the infiltrating immune cells are likely to be protective cells responding to the insult, but many are irrelevant bystanders. An EBV-infected, autoreactive B cell that enters the parenchyma in these circumstances will recognize and capture antigen and respond to this strong stimulus not by dying, as a naive B cell would, but by expressing LMP1, surviving and secreting antibody. Not all antibodies will be pathogenic, but only those that interfere with the function of some critical molecule or activate

Figure 6. Effector mechanisms and clinical consequences of LMP1-dependent demyelination

(A–E) Impact of MOG-reactive B cells with or without LMP1 expression on CNS myelin. (A) Fluorescent micrographs of striatal myelin. Yellow asterisk shows demyelinated area. Scale bar, 50 μm. (B–E) Quantitative figures related to (A); horizontal axes labeled BCR "M" (MOG-specific) or "P" (polyclonal). (B) Numbers of B cells. $^{****}p < 0.0001$; $^{***}p = 0.0002$; Kruskal-Wallis and Dunn's tests. (C) Quantification of demyelinated areas. Analyzed areas are represented in Figure S5E. $^{****}p < 0.0001$, one-way ANOVA with Dunnett's test. (D) C1q deposition around lesions. Exemplary image shown in Figure S5F. $^{*}p = 0.0394$; Kruskal-Wallis test followed by Dunn's tests. (E) C3d deposition around lesions. Exemplary image shown in Figure S5G. $^{*}p = 0.0246$; $^{***}p = 0.0005$; Kruskal-Wallis test followed by Dunn's tests.

(F–H) Interaction of LMP1-expressing, MOG-reactive B cells with naive 2D2 T cells. (F) Lateral motor deficit caused by B and T cell-induced lesion over 21 days. $^{†}p = 0.0690$, one-way ANOVA followed by Dunnett's test. (G and H) Quantitative figures related to (F); horizontal axes labeled TCR "M" (MOG-specific). (G) Numbers of B cells in the brains of mice from (F) at 16 and 21 days. $^{*}p = 0.0280$; $^{**}p = 0.0021$. (H) Numbers of $CD4^+$ T cells in the brains of mice from (F) at 16 and 21 days. $^{*}p = 0.0222$; $^{**}p = 0.0034$.

(I–K) MOG-reactive B cells in the healthy human repertoire. (I) Frequencies of MOG- and virus-reactive B cells in healthy humans. For one donor, B cells that captured SARS-CoV-2 spike protein were sorted and cultured in parallel, and for this donor, MOG-specific and spike-specific cells were subjected to scRNA-seq, and monoclonal antibodies were generated to confirm specificity and somatic hypermutation. Lower boxes indicate average frequencies of the two B cell populations; pie charts indicate immunoglobulin classes. (J) MOG specificity of an antibody cloned from a single B cell from a healthy human donor. See also Figure S5I. (K) Somatic hypermutation of immunoglobulin genes encoding MOG- and spike-specific antibodies. Colors indicate numbers of mutated nucleotides in heavy (HC) and light chains (LC). $^{***}p = 0.001$, Mann-Whitney test).

(L) Two-color immunohistochemical labeling of LMP1 (brown) and CD20 (red) in MS lesions. Paraffin sections of human brain biopsy tissue containing lesions were immunolabeled to reveal LMP1 expression and colocalization with the B cell marker CD20. An EBV-positive lymphoma sample was used as a positive control. Scale bar, 50 μm. See also Figures S5J and S5K. Donor information is provided in Table S1. All bars indicate means; error bars indicate standard deviation.

See also Figure S5.

some effector mechanism such as the complement cascade. Plasma cell differentiation in EBV-infected cells is associated with viral reactivation, after which elimination by cytotoxic T cells is likely in healthy individuals.[42] This viral control may be reduced in MS patients due to their specific genetic risk profile.[43] Several studies indicate an altered and probably insufficient anti-EBV response in MS patients, which could lead to a longer survival of EBV reactivating B cells.[43,44] Since most healthy individuals both have autoreactive naive B cells and are infected with EBV, the limiting constellation of events determining MS occurrence is likely to be EBV-induced clonal expansion of a B cell of the relevant specificity in combination with an insult leading to elevated CNS B cell invasion. The recently reported propensity of EBV-infected B cells to home to the CNS[45] would increase the probability that rare, myelin-reactive, EBV-infected cells encounter antigen in tissue and initiate lesion formation.

Rescue of antigen-capturing B cells by EBV would, of course, also be relevant for the antigen-presentation hypothesis, in that the longer a B cell survives after antigen capture, the higher the probability that it encounters a cognate T cell, and we observed more activated 2D2 T cells in the brains of mice that also had LMP1-expressing, MOG-reactive B cells in the brain. An alternative route to T cell activation, which fits well with our observation that microglial depletion reduces demyelination in this model, is that antibody-dependent phagocytosis facilitates antigen presentation by infiltrating myeloid cells or by microglia. Since myelin-reactive B and T cells are not frequent,[3] the probability that cognate cells encounter one another in the lymphocyte-poor conditions of the CNS is low, whereas the encounter between T cells and antigen-loaded phagocytes in the context of nascent lesion are more likely. Although there appears to be bidirectional traffic between the cerebrospinal fluid and the blood,[46] there is no compelling evidence that lymphocytes, once having entered the CNS parenchyma, ever leave it.[47] This poses a challenge for the idea that B cells could load antigen and traffic out to stimulate T cells, or that T cells, once activated in the brain, could traffic out to initiate additional independent lesions. Antigen presentation by myeloid cells via Fc receptor–dependent uptake of antibody-tagged antigens is well established experimentally in the context of EAE,[48,49] and interactions between myeloid cells and T cells are considered likely contributors to MS pathology.[50]

The question of how often EBV-infected B cells are found in the CNS in MS is controversial.[37–40,51] The model we describe requires that EBV-infected B cells come into contact with the brain parenchyma. However, they need not be abundant, perhaps not many more than one per lesion, and they might only survive for as long as the actively expanding phase of the lesion, so that failure to observe them is a probable outcome.

Other than depleting the EBV-infected pool by global B cell depletion, possible interventions targeting EBV to prevent or treat MS are increasingly being examined.[52,53] Our model predicts that an effective EBV vaccine would prevent MS, but also that interventions that induce lytic reactivation, and therefore immune clearance of latently infected cells, would reduce relapses in the long term, possibly at the cost of precipitating more lesions acutely. Notably, a vaccine that reduced the severity of an EBV infection and limited the maximum expansion of infected B cell clones could still reduce MS incidence, even without completely preventing infection.

The findings we report also have implications for basic B cell biology. We focused on the CNS, where immune cell ingress is restricted and opportunities for immune cell egress and traffic to secondary lymphoid organs are minimal,[49,50] but in organs such as the lung, with a large B cell population and free traffic to and from the lymphatic system, there is clearly potential for naive B cells to act as antigen scouts in infected tissue, in a manner similar to migratory dendritic cells.

In summary, we present a model of lesion initiation in MS centered on EBV-infected, myelin-reactive B cells in the context of non-autoimmune-mediated immune cell infiltration. This model explains how certain prodromes such as CNS infection and head trauma can increase the risk of MS, and it strengthens the rationale for a clinical vaccination trial aimed at preventing or ameliorating EBV infection in adolescents to reduce the risk of MS.

Limitations of the study

There are important differences between the experimental systems we describe and the physiological situation in humans. Most importantly, B cells transgenically expressing LMP1 lack many of the characteristics of EBV-infected human B cells, such as longevity and immune evasion. In EBV-infected human B cells, LMP1 is expressed only in concert with other viral genes that modify its effects,[51] and in the model we propose, it may be induced only by BCR stimulation.[54] The VSV infection we used also differs from a physiological infection in being replication-deficient and restricted to one location, which limits lesion formation in time and space. Although the model of lesion initiation by autoreactive, LMP1-expressing B cells can explain how MS relapses are prevented by B cell depletion and why they only occur in EBV-infected individuals, it does not directly explain the association of disease incidence with human leukocyte antigen (HLA) allotypes, which strongly indicates the involvement of T cells at some stage. It therefore seems likely that the pathogenesis of MS is a multi-step process that may be initiated by the mechanism we describe but probably involves other pathomechanisms in the course of disease progression.

RESOURCE AVAILABILITY

Lead contact

Further information and requests for resources and reagents should be directed to and will be fulfilled by the lead contact, Nicholas Sanderson (nicholas.sanderson@unibas.ch).

Materials availability

Plasmids and other materials generated in the study are available upon request from the lead contact.

Data and code availability

- Single-cell RNA-seq data have been deposited at GEO: GSE308213.
- Immunoglobulin gene sequences are available at NCBI nucleotide with accession numbers GenBank: PQ879402.1–PQ879429.1.
- All original code is publicly available at GitHub: https://github.com/julien-roux/Kim_Schneider_et_al_B_cells_expressing_EBV_LMP1_paper.

- Any additional information required is available from the lead contact upon request.

ACKNOWLEDGMENTS

We thank Daniel Pinschewer of the University of Basel for providing the L7 and V10 mice and for technical guidance for virus experiments, as well as Deniz Kaymak and Gregor Hutter of the University of Basel for providing mice and advice related to microglia depletion. We are grateful for technical support from the Microscopy, Bioinformatics, and Flow Cytometry Cores of the Department of Biomedicine, University of Basel; the Animal Research Station of the University of Basel; the BSSE; the University of Basel Scientific Computing Center (http://scicore.unibas.ch/); sequencing services from the Genomics Facility Basel D-BSSE; and the Egli group at the University of Zurich. Funding was received from the Swiss National Science Foundation (grants 169674, 189043, 10001495, and 10000065).

AUTHOR CONTRIBUTIONS

Conceptualization, H.K., M.S., J.R., N.S.R.S., M.D., and T.D.; methodology, H.K., M.S., P.K., J.R., G.P., E.B.-K., and N.S.R.S.; investigation, H.K., M.S., P.K., S.H., L. Kulsvehagen., A.-C.L., K.N., and R.S.; writing – original draft, H.K., M.S., J.R., N.S.R.S., and T.D.; funding acquisition, G.Z., A.-K.P., M.P., L. Kappos., N.S.R.S., and T.D.; resources, J.K. and G.Z.; supervision, A.-K.P., G.Z., N.S.R.S., and T.D.

DECLARATION OF INTERESTS

The authors declare no competing interests.

STAR★METHODS

Detailed methods are provided in the online version of this paper and include the following:

SUPPLEMENTAL INFORMATION

Supplemental information can be found online at https://doi.org/10.1016/j.cell.2025.12.031.

Received: January 15, 2025
Revised: September 18, 2025
Accepted: December 18, 2025
Published: January 13, 2026

REFERENCES

1. Comi, G., Bar-Or, A., Lassmann, H., Uccelli, A., Hartung, H.-P., Montalban, X., Sørensen, P.S., Hohlfeld, R., and Hauser, S.L.; Expert Panel of the 27th Annual Meeting of the European Charcot Foundation (2021). Role of B Cells in Multiple Sclerosis and Related Disorders. Ann. Neurol. *89*, 13–23. https://doi.org/10.1002/ana.25927.
2. Machado-Santos, J., Saji, E., Tröscher, A.R., Paunovic, M., Liblau, R., Gabriely, G., Bien, C.G., Bauer, J., and Lassmann, H. (2018). The compartmentalized inflammatory response in the multiple sclerosis brain is composed of tissue-resident CD8+ T lymphocytes and B cells. Brain *141*, 2066–2082. https://doi.org/10.1093/brain/awy151.
3. Hohlfeld, R., Dornmair, K., Meinl, E., and Wekerle, H. (2016). The search for the target antigens of multiple sclerosis, part 1: autoreactive CD4+ T lymphocytes as pathogenic effectors and therapeutic targets. Lancet Neurol. *15*, 198–209. https://doi.org/10.1016/S1474-4422(15)00334-8.
4. Ramaglia, V., Rojas, O., Naouar, I., and Gommerman, J.L. (2021). The Ins and Outs of Central Nervous System Inflammation-Lessons Learned from Multiple Sclerosis. Annu. Rev. Immunol. *39*, 199–226. https://doi.org/10.1146/annurev-immunol-093019-124155.
5. Molnarfi, N., Schulze-Topphoff, U., Weber, M.S., Patarroyo, J.C., Prod'homme, T., Varrin-Doyer, M., Shetty, A., Linington, C., Slavin, A.J., Hidalgo, J., et al. (2013). MHC class II-dependent B cell APC function is required for induction of CNS autoimmunity independent of myelin-specific antibodies. J. Exp. Med. *210*, 2921–2937. https://doi.org/10.1084/jem.20130699.
6. Zamvil, S.S., and Hauser, S.L. (2021). Antigen Presentation by B Cells in Multiple Sclerosis. N. Engl. J. Med. *384*, 378–381. https://doi.org/10.1056/NEJMcibr2032177.
7. Cyster, J.G. (2010). B cell follicles and antigen encounters of the third kind. Nat. Immunol. *11*, 989–996. https://doi.org/10.1038/ni.1946.
8. Lanzavecchia, A. (1985). Antigen-specific interaction between T and B cells. Nature *314*, 537–539. https://doi.org/10.1038/314537a0.
9. Meier, S., Willemse, E.A.J., Schaedelin, S., Oechtering, J., Lorscheider, J., Melie-Garcia, L., Cagol, A., Barakovic, M., Galbusera, R., Subramaniam, S., et al. (2023). Serum Glial Fibrillary Acidic Protein Compared With Neurofilament Light Chain as a Biomarker for Disease Progression in Multiple Sclerosis. JAMA Neurol. *80*, 287–297. https://doi.org/10.1001/jamaneurol.2022.5250.
10. Spillane, K.M., and Tolar, P. (2018). Mechanics of antigen extraction in the B cell synapse. Mol. Immunol. *101*, 319–328. https://doi.org/10.1016/j.molimm.2018.07.018.
11. Sanderson, N.S.R., Zimmermann, M., Eilinger, L., Gubser, C., Schaeren-Wiemers, N., Lindberg, R.L.P., Dougan, S.K., Ploegh, H.L., Kappos, L., and Derfuss, T. (2017). Cocapture of cognate and bystander antigens can activate autoreactive B cells. Proc. Natl. Acad. Sci. USA *114*, 734–739. https://doi.org/10.1073/pnas.1614472114.
12. Batista, F.D., Iber, D., and Neuberger, M.S. (2001). B cells acquire antigen from target cells after synapse formation. Nature *411*, 489–494. https://doi.org/10.1038/35078099.

13. Yuseff, M.-I., Pierobon, P., Reversat, A., and Lennon-Duménil, A.-M. (2013). How B cells capture, process and present antigens: a crucial role for cell polarity. Nat. Rev. Immunol. *13*, 475–486. https://doi.org/10.1038/nri3469.

14. Hedström, A.K. (2023). Risk factors for multiple sclerosis in the context of Epstein-Barr virus infection. Front. Immunol. *14*, 1212676. https://doi.org/10.3389/fimmu.2023.1212676.

15. Olsson, T., Barcellos, L.F., and Alfredsson, L. (2017). Interactions between genetic, lifestyle and environmental risk factors for multiple sclerosis. Nat. Rev. Neurol. *13*, 25–36. https://doi.org/10.1038/nrneurol.2016.187.

16. Bjornevik, K., Cortese, M., Healy, B.C., Kuhle, J., Mina, M.J., Leng, Y., Elledge, S.J., Niebuhr, D.W., Scher, A.I., Munger, K.L., et al. (2022). Longitudinal analysis reveals high prevalence of Epstein-Barr virus associated with multiple sclerosis. Science *375*, 296–301. https://doi.org/10.1126/science.abj8222.

17. Anderson, K.G., Mayer-Barber, K., Sung, H., Beura, L., James, B.R., Taylor, J.J., Qunaj, L., Griffith, T.S., Vezys, V., Barber, D.L., et al. (2014). Intravascular staining for discrimination of vascular and tissue leukocytes. Nat. Protoc. *9*, 209–222. https://doi.org/10.1038/nprot.2014.005.

18. Brioschi, S., Wang, W.-L., Peng, V., Wang, M., Shchukina, I., Greenberg, Z.J., Bando, J.K., Jaeger, N., Czepielewski, R.S., Swain, A., et al. (2021). Heterogeneity of meningeal B cells reveals a lymphopoietic niche at the CNS borders. Science *373*, eabf9277. https://doi.org/10.1126/science.abf9277.

19. Dougan, S.K., Ashour, J., Karssemeijer, R.A., Popp, M.W., Avalos, A.M., Barisa, M., Altenburg, A.F., Ingram, J.R., Cragnolini, J.J., Guo, C., et al. (2013). Antigen-specific B-cell receptor sensitizes B cells to infection by influenza virus. Nature *503*, 406–409. https://doi.org/10.1038/nature12637.

20. DiSano, K.D., Stohlman, S.A., and Bergmann, C.C. (2017). Activated GL7+ B cells are maintained within the inflamed CNS in the absence of follicle formation during viral encephalomyelitis. Brain Behav. Immun. *60*, 71–83. https://doi.org/10.1016/j.bbi.2016.09.022.

21. Metcalf, T.U., Baxter, V.K., Nilaratanakul, V., and Griffin, D.E. (2013). Recruitment and retention of B cells in the central nervous system in response to alphavirus encephalomyelitis. J. Virol. *87*, 2420–2429. https://doi.org/10.1128/JVI.01769-12.

22. Grut, V., Biström, M., Salzer, J., Stridh, P., Jons, D., Gustafsson, R., Fogdell-Hahn, A., Huang, J., Butt, J., Lindam, A., et al. (2024). Human herpesvirus 6A and axonal injury before the clinical onset of multiple sclerosis. Brain *147*, 177–185. https://doi.org/10.1093/brain/awad374.

23. Xu, Y., Smith, K.A., Hiyoshi, A., Piehl, F., Olsson, T., and Montgomery, S. (2021). Hospital-diagnosed infections before age 20 and risk of a subsequent multiple sclerosis diagnosis. Brain *144*, 2390–2400. https://doi.org/10.1093/brain/awab100.

24. Florova, M., Abreu-Mota, T., Paesen, G.C., Beetschen, A.S., Cornille, K., Marx, A.-F., Narr, K., Sahin, M., Dimitrova, M., Swarnalekha, N., et al. (2024). Central tolerance shapes the neutralizing B cell repertoire against a persisting virus in its natural host. Proc. Natl. Acad. Sci. USA *121*, e2318657121. https://doi.org/10.1073/pnas.2318657121.

25. Maloy, K.J., Burkhart, C., Freer, G., Rülicke, T., Pircher, H., Kono, D.H., Theofilopoulos, A.N., Ludewig, B., Hoffmann-Rohrer, U., Zinkernagel, R.M., et al. (1999). Qualitative and quantitative requirements for CD4+ T cell-mediated antiviral protection. J. Immunol. *162*, 2867–2874. https://doi.org/10.4049/jimmunol.162.5.2867.

26. Litzenburger, T., Fässler, R., Bauer, J., Lassmann, H., Linington, C., Wekerle, H., and Iglesias, A. (1998). B lymphocytes producing demyelinating autoantibodies: development and function in gene-targeted transgenic mice. J. Exp. Med. *188*, 169–180. https://doi.org/10.1084/jem.188.1.169.

27. Akkaya, M., Traba, J., Roesler, A.S., Miozzo, P., Akkaya, B., Theall, B.P., Sohn, H., Pena, M., Smelkinson, M., Kabat, J., et al. (2018). Second signals rescue B cells from activation-induced mitochondrial dysfunction and death. Nat. Immunol. *19*, 871–884. https://doi.org/10.1038/s41590-018-0156-5.

28. Münchhalfen, M., Görg, R., Haberl, M., Löber, J., Willenbrink, J., Schwarzt, L., Höltermann, C., Ickes, C., Hammermann, L., Kus, J., et al. (2024). TFEB activation hallmarks antigenic experience of B lymphocytes and directs germinal center fate decisions. Nat. Commun. *15*, 6971. https://doi.org/10.1038/s41467-024-51166-3.

29. Haghayegh Jahromi, N., Marchetti, L., Moalli, F., Duc, D., Basso, C., Tardent, H., Kaba, E., Deutsch, U., Pot, C., Sallusto, F., et al. (2019). Intercellular Adhesion Molecule-1 (ICAM-1) and ICAM-2 Differentially Contribute to Peripheral Activation and CNS Entry of Autoaggressive Th1 and Th17 Cells in Experimental Autoimmune Encephalomyelitis. Front. Immunol. *10*, 3056. https://doi.org/10.3389/fimmu.2019.03056.

30. Mintz, M.A., and Cyster, J.G. (2020). T follicular helper cells in germinal center B cell selection and lymphomagenesis. Immunol. Rev. *296*, 48–61. https://doi.org/10.1111/imr.12860.

31. Thorley-Lawson, D.A. (2015). EBV Persistence–Introducing the Virus. Curr. Top. Microbiol. Immunol. *390*, 151–209. https://doi.org/10.1007/978-3-319-22822-8_8.

32. Kaye, K.M., Izumi, K.M., and Kieff, E. (1993). Epstein-Barr virus latent membrane protein 1 is essential for B-lymphocyte growth transformation. Proc. Natl. Acad. Sci. USA *90*, 9150–9154. https://doi.org/10.1073/pnas.90.19.9150.

33. Yuan, J., Cahir-McFarland, E., Zhao, B., and Kieff, E. (2006). Virus and cell RNAs expressed during Epstein-Barr virus replication. J. Virol. *80*, 2548–2565. https://doi.org/10.1128/JVI.80.5.2548-2565.2006.

34. Ciucci, M.R., Ma, S.T., Kane, J.R., Ahrens, A.M., and Schallert, T. (2008). Limb use and complex ultrasonic vocalization in a rat model of Parkinson's disease: deficit-targeted training. Parkinsonism Relat. Disord. *14*, S172–S175. https://doi.org/10.1016/j.parkreldis.2008.04.027.

35. Rose, N., Holdermann, S., Callegari, I., Kim, H., Fruh, I., Kappos, L., Kuhle, J., Müller, M., Sanderson, N.S.R., and Derfuss, T. (2022). Receptor clustering and pathogenic complement activation in myasthenia gravis depend on synergy between antibodies with multiple subunit specificities. Acta Neuropathol. *144*, 1005–1025. https://doi.org/10.1007/s00401-022-02493-6.

36. Callegari, I., Schneider, M., Berloffa, G., Mühlethaler, T., Holdermann, S., Galli, E., Roloff, T., Boss, R., Infanti, L., Khanna, N., et al. (2022). Potent neutralization by monoclonal human IgM against SARS-CoV-2 is impaired by class switch. EMBO Rep. *23*, e53956. https://doi.org/10.15252/embr.202153956.

37. Orr, N., and Steinman, L. (2025). Epstein-Barr virus and the immune microenvironment in multiple sclerosis: Insights from high-dimensional brain tissue imaging. Proc. Natl. Acad. Sci. USA *122*, e2425670122. https://doi.org/10.1073/pnas.2425670122.

38. Moreno, M.A., Or-Geva, N., Aftab, B.T., Khanna, R., Croze, E., Steinman, L., and Han, M.H. (2018). Molecular signature of Epstein-Barr virus infection in MS brain lesions. Neurol. Neuroimmunol. Neuroinflamm. *5*, e466. https://doi.org/10.1212/NXI.0000000000000466.

39. Serafini, B., Benincasa, L., Rosicarelli, B., and Aloisi, F. (2024). EBV infected cells in the multiple sclerosis brain express PD-L1: How the virus and its niche may escape immune surveillance. J. Neuroimmunol. *389*, 578314. https://doi.org/10.1016/j.jneuroim.2024.578314.

40. Lassmann, H., Niedobitek, G., Aloisi, F., and Middeldorp, J.M.; NeuroproMiSe; EBV Working Group (2011). Epstein-Barr virus in the multiple sclerosis brain: a controversial issue–report on a focused workshop held in the Centre for Brain Research of the Medical University of Vienna, Austria. Brain *134*, 2772–2786. https://doi.org/10.1093/brain/awr197.

41. Johansson, E., Alfredsson, L., Strid, P., Kockum, I., Olsson, T., and Hedström, A.K. (2024). Head trauma results in manyfold increased risk of multiple sclerosis in genetically susceptible individuals. J. Neurol. Neurosurg. Psychiatry *95*, 554–560. https://doi.org/10.1136/jnnp-2023-332643.

42. Laichalk, L.L., and Thorley-Lawson, D.A. (2005). Terminal differentiation into plasma cells initiates the replicative cycle of Epstein-Barr virus in vivo. J. Virol. *79*, 1296–1307. https://doi.org/10.1128/JVI.79.2.1296-1307.2005.

43. Zdimerova, H., Murer, A., Engelmann, C., Raykova, A., Deng, Y., Gujer, C., Rühl, J., McHugh, D., Caduff, N., Naghavian, R., et al. (2021). Attenuated immune control of Epstein-Barr virus in humanized mice is associated with the multiple sclerosis risk factor HLA-DR15. Eur. J. Immunol. *51*, 64–75. https://doi.org/10.1002/eji.202048655.

44. Hedström, A.K., Huang, J., Michel, A., Butt, J., Brenner, N., Hillert, J., Waterboer, T., Kockum, I., Olsson, T., and Alfredsson, L. (2019). High Levels of Epstein-Barr Virus Nuclear Antigen-1-Specific Antibodies and Infectious Mononucleosis Act Both Independently and Synergistically to Increase Multiple Sclerosis Risk. Front. Neurol. *10*, 1368. https://doi.org/10.3389/fneur.2019.01368.

45. Läderach, F., Piteros, I., Fennell, É., Bremer, E., Last, M., Schmid, S., Rieble, L., Campbell, C., Ludwig-Portugall, I., Bornemann, L., et al. (2025). EBV induces CNS homing of B cells attracting inflammatory T cells. Nature *646*, 171–179. https://doi.org/10.1038/s41586-025-09378-0.

46. von Büdingen, H.-C., Kuo, T.C., Sirota, M., van Belle, C.J., Apeltsin, L., Glanville, J., Cree, B.A., Gourraud, P.-A., Schwartzburg, A., Huerta, G., et al. (2012). B cell exchange across the blood-brain barrier in multiple sclerosis. J. Clin. Investig. *122*, 4533–4543. https://doi.org/10.1172/JCI63842.

47. Engelhardt, B., Vajkoczy, P., and Weller, R.O. (2017). The movers and shapers in immune privilege of the CNS. Nat. Immunol. *18*, 123–131. https://doi.org/10.1038/ni.3666.

48. Haimon, Z., Frumer, G.R., Kim, J.-S., Trzebanski, S., Haffner-Krausz, R., Ben-Dor, S., Porat, Z., Muschaweckh, A., Chappell-Maor, L., Boura-Halfon, S., et al. (2022). Cognate microglia-T cell interactions shape the functional regulatory T cell pool in experimental autoimmune encephalomyelitis pathology. Nat. Immunol. *23*, 1749–1762. https://doi.org/10.1038/s41590-022-01360-6.

49. Kinzel, S., Lehmann-Horn, K., Torke, S., Häusler, D., Winkler, A., Stadelmann, C., Payne, N., Feldmann, L., Saiz, A., Reindl, M., et al. (2016). Myelin-reactive antibodies initiate T cell-mediated CNS autoimmune disease by opsonization of endogenous antigen. Acta Neuropathol. *132*, 43–58. https://doi.org/10.1007/s00401-016-1559-8.

50. Charabati, M., Wheeler, M.A., Weiner, H.L., and Quintana, F.J. (2023). Multiple sclerosis: Neuroimmune crosstalk and therapeutic targeting. Cell *186*, 1309–1327. https://doi.org/10.1016/j.cell.2023.03.008.

51. Soldan, S.S., and Lieberman, P.M. (2023). Epstein-Barr virus and multiple sclerosis. Nat. Rev. Microbiol. *21*, 51–64. https://doi.org/10.1038/s41579-022-00770-5.

52. Aloisi, F., Giovannoni, G., and Salvetti, M. (2023). Epstein-Barr virus as a cause of multiple sclerosis: opportunities for prevention and therapy. Lancet Neurol. *22*, 338–349. https://doi.org/10.1016/S1474-4422(22)00471-9.

53. Pender, M.P., Csurhes, P.A., Smith, C., Douglas, N.L., Neller, M.A., Matthews, K.K., Beagley, L., Rehan, S., Crooks, P., Hopkins, T.J., et al. (2018). Epstein-Barr virus-specific T cell therapy for progressive multiple sclerosis. JCI Insight *3*, e124714. https://doi.org/10.1172/jci.insight.124714.

54. Lyu, L., Li, Q., and Wang, C. (2025). EBV Latency Programs: Molecular and Epigenetic Regulation and Its Role in Disease Pathogenesis. J. Med. Virol. *97*, e70501. https://doi.org/10.1002/jmv.70501.

55. Hoffmann, M., Wu, Y.-J., Gerber, M., Berger-Rentsch, M., Heimrich, B., Schwemmle, M., and Zimmer, G. (2010). Fusion-active glycoprotein G mediates the cytotoxicity of vesicular stomatitis virus M mutants lacking host shut-off activity. J. Gen. Virol. *91*, 2782–2793. https://doi.org/10.1099/vir.0.023978-0.

56. Berger-Rentsch, M., and Zimmer, G. (2011). A vesicular stomatitis virus replicon-based bioassay for the rapid and sensitive determination of multi-species type I interferon. PLOS One *6*, e25858. https://doi.org/10.1371/journal.pone.0025858.

57. Hanika, A., Larisch, B., Steinmann, E., Schwegmann-Weßels, C., Herrler, G., and Zimmer, G. (2005). Use of influenza C virus glycoprotein HEF for generation of vesicular stomatitis virus pseudotypes. J. Gen. Virol. *86*, 1455–1465. https://doi.org/10.1099/vir.0.80788-0.

58. Lou, E., Fujisawa, S., Morozov, A., Barlas, A., Romin, Y., Dogan, Y., Gholami, S., Moreira, A.L., Manova-Todorova, K., and Moore, M.A.S. (2012). Tunneling nanotubes provide a unique conduit for intercellular transfer of cellular contents in human malignant pleural mesothelioma. PLoS One *7*, e33093. https://doi.org/10.1371/journal.pone.0033093.

59. Presley, J.F., Cole, N.B., Schroer, T.A., Hirschberg, K., Zaal, K.J., and Lippincott-Schwartz, J. (1997). ER-to-Golgi transport visualized in living cells. Nature *389*, 81–85. https://doi.org/10.1038/38001.

60. Schindelin, J., Arganda-Carreras, I., Frise, E., Kaynig, V., Longair, M., Pietzsch, T., Preibisch, S., Rueden, C., Saalfeld, S., Schmid, B., et al. (2012). Fiji: an open-source platform for biological-image analysis. Nat. Methods. *9*, 676–682. https://doi.org/10.1038/nmeth.2019.

61. Bankhead, P., Loughrey, M.B., Fernández, J.A., Dombrowski, Y., McArt, D.G., Dunne, P.D., McQuaid, S., Gray, R.T., Murray, L.J., Coleman, H.G., et al. (2017). QuPath: Open source software for digital pathology image analysis. Sci. Rep. *7*, 16878. https://doi.org/10.1038/s41598-017-17204-5.

62. R Core Team (2021). R: A Language and Environment for Statistical Computing (Vienna: R Foundation for Statistical Computing). https://www.R-project.org.

63. Dobin, A., Davis, C.A., Schlesinger, F., Drenkow, J., Zaleski, C., Jha, S., Batut, P., Chaisson, M., and Gingeras, T.R. (2013). STAR: ultrafast universal RNA-seq aligner. Bioinformatics *29*, 15–21. https://doi.org/10.1093/bioinformatics/bts635.

64. Cadiñanos, J., and Bradley, A. (2007). Generation of an inducible and optimized piggyBac transposon system. Nucleic Acids Res. *35*, e87. https://doi.org/10.1093/nar/gkm446.

65. McInnes, L., Healy, J., and Melville, J. (2018). UMAP: Uniform Manifold Approximation and Projection for Dimension Reduction. Preprint at arXiv. https://doi.org/10.48550/ARXIV.1802.03426.

66. Van Gassen, S., Callebaut, B., Van Helden, M.J., Lambrecht, B.N., Demeester, P., Dhaene, T., and Saeys, Y. (2015). FlowSOM: Using self-organizing maps for visualization and interpretation of cytometry data. Cytometry A *87*, 636–645. https://doi.org/10.1002/cyto.a.22625.

67. Sieckmann, D.G., Stall, A.M., and Subbarao, B. (1991). A mouse monoclonal antibody specific for an allotypic determinant of the Igha allele of murine IgM: genetic and functional analysis of Igh-6a epitopes using anti-IgM monoclonal antibodies. Hybridoma *10*, 121–135. https://doi.org/10.1089/hyb.1991.10.121.

68. Lun, A.T.L., Riesenfeld, S., Andrews, T., Dao, T.P., Gomes, T., and Marioni, J.C. (2019). EmptyDrops: distinguishing cells from empty droplets in droplet-based single-cell RNA sequencing data. Genome Biol *20*, 63. https://doi.org/10.1186/s13059-019-1662-y.

69. Vallejos, C.A., Risso, D., Scialdone, A., Dudoit, S., and Marioni, J.C. (2017). Normalizing single-cell RNA sequencing data: challenges and opportunities. Nat. Methods. *14*, 565–571. https://doi.org/10.1038/nmeth.4292.

70. Lun, A.T., Bach, K., and Marioni, J.C. (2016). Pooling across cells to normalize single-cell RNA sequencing data with many zero counts. Genome Biol *17*, 75. https://doi.org/10.1186/s13059-016-0947-7.

71. McCarthy, D.J., Campbell, K.R., Lun, A.T., and Wills, Q.F. (2017). Scater: pre-processing, quality control, normalization and visualization of single-cell RNA-seq data in R. Bioinformatics *33*, 1179–1186. https://doi.org/10.1093/bioinformatics/btw777.

72. Amezquita, R.A., Lun, A.T.L., Becht, E., Carey, V.J., Carpp, L.N., Geistlinger, L., Marini, F., Rue-Albrecht, K., Risso, D., Soneson, C., et al. (2020). Orchestrating single-cell analysis with Bioconductor. Nat. Methods. *17*, 137–145. https://doi.org/10.1038/s41592-019-0654-x.

73. Germain, P.L., Lun, A., Garcia Meixide, C., Macnair, W., and Robinson, M.D. (2021). Doublet identification in single-cell sequencing data using *scDblFinder*. F1000Res. *10*, 979. https://doi.org/10.12688/f1000research.73600.2.

74. Aran, D., Looney, A.P., Liu, L., Wu, E., Fong, V., Hsu, A., Chak, S., Naikawadi, R.P., Wolters, P.J., Abate, A.R., et al. (2019). Reference-based analysis of lung single-cell sequencing reveals a transitional profibrotic macrophage. Nat. Immunol. *20*, 163–172. https://doi.org/10.1038/s41590-018-0276-y.

75. Haghverdi, L., Lun, A.T.L., Morgan, M.D., and Marioni, J.C. (2018). Batch effects in single-cell RNA-sequencing data are corrected by matching mutual nearest neighbors. Nat. Biotechnol. *36*, 421–427. https://doi.org/10.1038/nbt.4091.

76. Chen, Y., Chen, L., Lun, A.T.L., Baldoni, P.L., and Smyth, G.K. (2025). edgeR v4: powerful differential analysis of sequencing data with expanded functionality and improved support for small counts and larger datasets. Nucleic Acids Res. *53*, gkaf018. https://doi.org/10.1093/nar/gkaf018.

77. Sziber, Z., Torrents-Solé, P., Kovacevic, A., and Kapfhammer, J.P. (2025). Protein kinase C gamma regulates Purkinje cell dendritic spine development in a mouse model of spinocerebellar ataxia. Exp. Neurol. *393*, 115377. https://doi.org/10.1016/j.expneurol.2025.115377.

STAR★METHODS

KEY RESOURCES TABLE

REAGENT or RESOURCE	SOURCE	IDENTIFIER
Antibodies		
Alexa Fluor 700 anti-mouse CD3e	ThermoFisher	Cat#56-0033-82; RRID:AB_837094
Brilliant Violet 510 anti-mouse CD19	BioLegend	Cat#115545; RRID:AB_2562136
Brilliant Violet 421 anti-mouse CD20	BioLegend	Cat#150405; RRID:AB_2566540
Alexa Fluor 647 anti-mouse CD45	BioLegend	Cat#103124; RRID:AB_493533
Alexa Fluor 647 anti-mouse CD19	BioLegend	Cat# 115522 RRID:AB_389329
PerCP-Cy 5.5 anti-mouse CD45.2	BD Biosciences	Cat#552950; RRID:AB_394528
Brilliant Violet 605 anti-mouse CD68	Biolegend	Cat#137021; RRID:AB_2616811
Brilliant Violet 711 anti-mouse/human CD45R/B220	BioLegend	Cat#103255; RRID:AB_2563491
PE/Dazzle 594 anti-mouse CD138 (Syndecan-1)	BioLegend	Cat#142528; RRID:AB_2566495
APC/Cy7 anti-mouse F4/80	BioLegend	Cat#123118; RRID:AB_893477
Alexa Fluor 488 anti-mouse IgM, μ Chain Specific	Jackson ImmunoResearch	Cat#715-545-020; RRID:AB_2340844
PerCP-Cy5.5 anti-mouse CD69	BD Bioscience	Cat#551113; RRID:AB_394051
APC goat anti-human IgG	Jackson ImmunoResearch	Cat#109-135-098; RRID:AB_2337690
Cell Trace Violet	Invitrogen	Cat#C34557
Rabbit anti-MOG mAb (E5K6T)	Cell signaling technology	Cat#96457; RRID:AB_ 2800265
Rabbit anti-GFAP mAb (E4L7M)	Cell signaling technology	Cat#80788; RRID:AB_2799963
Rabbit anti-NeuN mAb (D3S3I)	Cell signaling technology	Cat#1294; RRID:AB_ 2630395
Rat anti-MBP	Sigma-Aldrich	Cat#MAB386; RRID:AB_94975
Chicken anti-Neurofilament	Abcam	Cat#24520; RRID:AB_726986
PE/Cy7 anti-mouse CD154 (CD40L)	BioLegend	Cat#157008; RRID:AB_2832545
Rabbit anti-Laminin	Abcam	Cat#Ab11575; RRID:AB_298179
Rabbit anti-influenza HA	Sino Biological	Cat#11692-T62; RRID:AB_3676976
Alexa Fluor 647 goat anti-rabbit IgG(H+L)	Jackson Immunoresearch	Cat#111-605-003; RRID:AB_2338072
Alexa Fluor 647 donkey anti-rat IgG(H+L)	Jackson Immunoresearch	Cat#712-605-153; RRID:AB_2340694
FITC goat anti-rat IgG(H+L)	Jackson Immunoresearch	Cat#112-095-167; RRID:AB_2338200
Rhodamine Red-X (RXX) AffiniPure goat anti-mouse IgG (H+L)	Jackson Immunoresearch	Cat#115-295-166; RRID: AB_2338768
Alexa Fluor 488 anti-mouse IgG2b	Jackson Immunoresearch	Cat#115-545-207; RRID:AB_2338856
Rat anti-CD3	Invitrogen	Cat#14-0032-86; RRID:AB_467055
Anti-C1q antibody (7H8)	Abcam	Cat#ab11861; RRID:AB_298643
Brilliant Violet 605 rat anti-mouse CD19	BD Bioscience	Cat#563148; RRID:AB_2732057
Alexa Fluor 647 anti-mouse CD45R (B220)	BioLegend	Cat#103226; RRID:AB_389330
Alexa Fluor 700 anti-mouse CD3e	BioLegend	Cat#152316; RRID:AB_2632713
APC/Cy7 anti-mouse CD25	BioLegend	Cat#101918; RRID:AB_2650982
Streptavidin-HRP	Jackson Immunoresearch	Cat#016-030-084; RRID:AB_2337238
TotalSeq-C0301 anti-mouse Hashtag 1 antibody solution	BioLegend	Cat#155861; RRID:AB_2800693
Chicken anti-MBP	Invitrogen	Cat#PA1-10008; RRID:AB_1077024
Brilliant Ultra Violet 395 anti mouse CD45	BD Biosciences	Cat#567451; RRID:AB_2916597
Brilliant Ultra Violet 496 anti-mouse CD4	BD Biosciences	Cat#612952; RRID:AB_2813886
Brilliant Ultra Violet 661 anti-mouse CD19	BD Biosciences	Cat#612971; RRID:AB_2870243

(*Continued on next page*)

Continued

REAGENT or RESOURCE	SOURCE	IDENTIFIER
Brilliant Ultra Violet 737 anti-mouse CD62L (L-Selectin)	BD Biosciences	Cat#612833; RRID:AB_2870155
Brilliant Ultra Violet 805 anti-mouse CD8a	BD Biosciences	Cat#612898; RRID:AB_2870186
Brilliant Violet 480 anti-mouse Ki-67	BD Biosciences	Cat#566172; RRID:AB_2739569
Brilliant Violet 605 anti-mouse CX3CR1	BioLegend	Cat#149027; RRID:AB_2565937
Brilliant Violet 711 anti-mouse/human B220	BioLegend	Cat#103255; RRID:AB_2563491
Brilliant Violet 785 anti-mouse/human CD44	BioLegend	Cat#103041; RRID:AB_11218802
FITC anti-mouse TCR Va3.2	BioLegend	Cat#135403; RRID:AB_1937236
FITC anti-mouse IgM[a]	BD Biosciences	Cat#553516; RRID:AB_394897
PerCP-Cy5.5 anti-mouse TCR beta	BioLegend	Cat#109227; RRID:AB_1575176
PerCP-Fire806 anti-mouse I-A/I-E	BioLegend	Cat#107673; RRID:AB_2941380
PE anti-mouse P2RY12	BioLegend	Cat#848003; RRID:AB_2721644
PE-Dazzle594 anti-mouse CD186 (CXCR6)	BioLegend	Cat#151116; RRID:AB_2721699
PE-Cy5 anti-mouse CD45	BioLegend	Cat#103109; RRID:AB_312974
PE-Cy7 anti-mouse CD40	BioLegend	Cat#124621; RRID:AB_10933422
APC anti-mouse CD369 (CLEC7a)	BioLegend	Cat#144305; RRID:AB_2616699
Spark R718 anti-mouse CD69	BioLegend	Cat#104559; RRID:AB_2924442
APC-Fire810 anti-mouse/human CD11b	BioLegend	Cat#101287; RRID:AB_2910274
Brilliant Violet 421 anti-mouse IL-17A	BioLegend	Cat#506925; RRID:AB_10900442
Brilliant Violet 605 anti-mouse IL-2	BioLegend	Cat#503829; RRID:AB_11204084
PE anti-mouse IL-10	BioLegend	Cat#505007; RRID:AB_315361
PE-Cy7 anti-mouse IFN-γ	BioLegend	Cat#505825; RRID:AB_1595591
APC anti-mouse GM-CSF	BioLegend	Cat#505413; RRID:AB_2721460
Rabbit anti-NEFL	Invitrogen	Cat#MA5-14981; RRID:AB_10984147
DAPI	Sigma-Aldrich	Cat#D9542
Brilliant Violet 785 anti-human CD69	BioLegend	Cat#310931; RRID:AB_2561370
F(ab')2 donkey anti-mouse IgM	Jackson ImmunoResearch	Cat#715-006-020; RRID:AB_2340760
Purified anti-mouse CD28	BioLegend	Cat# 102101; RRID:AB_312866
EBV LMP-1 antibody (3H2104a,b,c)	Santa Cruz Biotechnology	Cat#sc-71023; RRID:AB_1122589
FLEX mouse anti-human CD20cy (ready-to-use)	Agilent	Cat#IR604; RRID:AB_3075456
Bacterial and virus strains		
Influenza A/WSN/1933 (H1N1)	ATCC	Cat#VR-1520
AVV-vPigLIC-CD40L	This paper	N/A
VSV*ΔG	Hoffmann et al.[55]	N/A
VSV-G*	Berger-Rentsch and Zimmer[56]	N/A
Stellar competent cells (E. coli HST08 strain)	Takara	Cat#636763
Biological samples		
Blood from human donors	Ethical committee of Northwest Switzerland	EKNZ project ID 2021-00961
Brain biopsies and autopsies	Freiburg Ethics Commission	N/A
Chemicals, peptides, and recombinant proteins		
Dulbecco's PBS without Ca++/Mg++	BioConcept	Cat#3-05F29-I
Corn oil	Sigma-Aldrich	Cat#C8267; CAS-No: 8001-30-7
Yeast Extract	Millipore	Cat#92144; CAS-No: 8013-01-2
LB Agar	Sigma-Aldrich	Cat#L7025
Fluoromount-G	SouthernBiotech	Cat#0100-01
EDTA disodium salt dihydrate	Sigma-Aldrich	Cat#E5134; CAS-No: 6381-92-6
Triton X-100	Sigma-Aldrich	Cat#X100; CAS-No: 9002-93-1

(*Continued on next page*)

Continued

REAGENT or RESOURCE	SOURCE	IDENTIFIER
NaCl 0.9 % solution	B. Braun Medical AG	Cat#395202
TopVision Low Melting Point Agarose	Thermo Scientific	Cat#R0801
EDTA	Sigma-Aldrich	Cat#EDS; CAS-No: 60-00-4
Glycerol	Sigma-Aldrich	Cat#G5516; CAS-No: 56-81-5
Glycine	Sigma-Aldrich	Cat#G7126; CAS-No: 56-40-6
HEPES	Sigma-Aldrich	Cat#H3375 CAS-No: 7365-45-9
Saponin	Sigma-Aldrich	Cat#84510; CAS-No: 8047-15-2
Sodium azide	Sigma-Aldrich	Cat#S2002; CAS-No: 26628-22-8
Tamoxifen	Sigma-Aldrich	Cat#T5648; CAS-No: 10540-29-1
Acetic acid, >99%	Sigma-Aldrich	Cat#A6283; CAS-No: 64-19-7
Sodium hydroxide, 1N	Acros Organics	Cat#124260010; CAS-No: 1310-73-2
Hydrochloric acid, 2.0 mol/l	Sigma-Aldrich	Cat#35327; CAS-No: 7647-01-0
Paraformaldehyde	Sigma-Aldrich	Cat#P6148; CAS-No: 30525-89-4
Fetal Bovine Serum	Biowest	Cat#S1810-500; CAS-No: S00CJ
Citric acid monohydrate	Sigma-Aldrich	Cat#C7129; CAS-No: 5949-29-1
Biotinylated Lycopersicon esculentum lectin	AdipoGen	Cat#VC-B-1175-M001
Sodium citrate tribasic dihydrate	Sigma-Aldrich	Cat#C0909; CAS-No: 6132-04-3
Nuclease-free Water	BioLabs	Cat#B1500S
Ammonium chloride	Fluka BioChemika	Cat#09718;
Sodium bicarbonate	Sigma-Aldrich	Cat#792519; CAS-No: 144-55-8
DMSO	Life technologies	Cat#L34964
Trypsin EDTA without Ca++/Mg++	Bioconcept	Cat#5-51F00-H
RPMI 1640 with L glutamate	Bioconcept	Cat#1-41F03-I
DMEM High Glucose with L-Glutamine	BioConcept	Cat#1-26F03-1
Hank's BSS (HBSS)	Bioconcept	Cat#3-02F00-I
2-Mercaptoethanol	Sigma-Aldrich	Cat#M7522; CAS-No: 60-24-2
Penicillin Streptomycin	Bioconcept	Cat#4-01F00-H
Puromycin	Gibco	Cat#A11138-03
Trypan Blue solution	Sigma-Aldrich	Cat#93595; CAS-No:72-57-1
Lymphoprep	Serumwerk Bernburg	Cat#04-03-9391/03
Liberase	Roche	Cat#05401127001
DNase I	Sigma-Aldrich	Cat#A3778; CAS-No: 9003-98-9
Ampicillin sodium salt	Sigma-Aldrich	Cat#A9518; CAS-No: 69-52-3
Geneticin	Gibco	Cat#10131-035
jetPRIME buffer	Polyplus	Cat#201000003
jetPRIME transfection reagent	Polyplus	Cat#101000015
OptiMEM	Sigma-Aldrich	Cat#M0268
PaC I	BioLabs	Cat#R0547L
rCutSmart buffer	BioLabs	Cat#B6004S
TE buffer	Ambion	Cat#AM9861
SOC medium	Takara	Cat#ST0215
Tryptone	Sigma-Aldrich	Cat#95039
Agarose	Sigma-Aldrich	Cat#A9539
Sodium chloride	Sigma-Aldrich	Cat#S7653
Collagenase	Thermo Fisher	Cat#17104019
L-Glutamine	BioConcept	Cat#1-31S01-I
Tween-20	Sigma-Aldrich	Cat#P1379
3-amino-9-ethyl-carbazole (AEC)	Sigma-Aldrich	Cat#A5754; CAS-No:132-32-1

(*Continued on next page*)

Continued

REAGENT or RESOURCE	SOURCE	IDENTIFIER
N,N-Dimethylformamide (DMF)	Fluka Analytical	Cat#40255
H2O2 (30 %)	CarlRoth	Cat#9681.4; CAS-No: 7722-84-1
Swa I	BioLabs	Cat#R0604S
dNTP	BioLabs	Cat#N0447S
Phusion Hot start Flex DNA polymerase	BioLabs	Cat#M0535S
5X Phusion HF buffer	BioLabs	Cat#B0518S
10x NEBuffer 2.1	BioLabs	Cat#B7202S
MgCl2	BioLabs	Cat#B9021S
DTT	Invitrogen	Cat#Y00147
T4 DNA polymerase	BioLabs	Cat#M0203L
dGTP	VWR Amresco	Cat#E539
dCTP	VWR Amresco	Cat#E536
CD45 microbeads	Miltenyi Biotec	Cat#130-052-301
SPRI select	Beckman Coulter	Cat#B23318
Dynabeads MyOne Silane	10X Genomics	Cat#2000048
BME	Gibco	Cat#21010-046
Horse Serum	Gibco	Cat#26050-088
Glutamax	Gibco	Cat#35050-061
Glucose 10%	Sigma	Cat#G8644
T4 DNA Ligase buffer	BioLabs	Cat#B0202A
Ionomycin calcium salt	Sigma-Aldrich	Cat#I0634; Cas-No: 56092-82-1
Phorbol 12-myristate 13-acetate	Sigma-Aldrich	Cat#P8139; Cas-No: 16561-29-8
True-Nuclear Transcription Factor Buffer Set	Biolegend	Cat#424401
Fixation Buffer	Biolegend	Cat#420801
Intracellular staining perm wash buffer (10x)	Biolegend	Cat#421002
Monensin Solution (1,000X)	Biolegend	Cat#420701
Brefeldin A Solution (1,000X)	Biolegend	Cat#420601
TruStain fcXPLUS (anti-mouse CD16/32)	Biolegend	Cat#156603
Zombie UV Fixable viability kit	Biolegend	Cat#423107
Cell staining buffer	Biolegend	Cat#420201
Percoll	Cytiva	Cat#17089102
Collagenase Type IV	Merck	Cat#C4-BIOC
DNase I	ITW Reagents	Cat#A3778; Cas-No: 9003-98-9
PLX5622	MCE	Cat#HY-114153; Cas-No: 1303420-67-8
Recombinant mouse IL-2	eBioscience	Cat#AF-212-12
Recombinant mouse IL-7	Peprotech	Cat#217-17
Recombinant mouse IL-12 p70	Peprotech	Cat#210-12
Recombinant mouse IL-18	Biozol	Cat#B002-5
Recombinant human IL-21	Gibco	Cat# PHC0215
MOG_{35-55}	ANASPEC	Cat#AS-60130-5
$OVA_{323-339}$	ANASPEC	Cat#AS-27024
Critical commercial assays		
Pan B cell isolation kit, mouse	Miltenyi Biotec	Cat#130-104-443
$CD4^+$ T cell isolation kit, mouse	Miltenyi Biotec	Cat#130-104-454
Pan B cell isolation kit, human	Miltenyi Biotec	Cat#130-101-638
VersaComp Antibody Capture Bead Kit	Beckman Coulter	Cat#B22804
Gel and PCR Clean-up	Macherey-Nagel	Cat#740609.250
NucleoSpin Plasmid	Macherey-Nagel	Cat#740588.250

(*Continued on next page*)

Continued

REAGENT or RESOURCE	SOURCE	IDENTIFIER
Zymo quick-RNA kit	Zymo Research	Cat#R1050
SMART-Seq v4 Ultra low input RNA kit	Takara	Cat#634888
Equinox Library Amplification kit	Watchmaker Genomics	Cat#7K0014-096
AVITI 2X75 Sequencing Kit Cloudbreak FS High Output	Element Biosciences	Cat#860-00015
DNA prep kit	Illumina	Cat#1000000025416
Xtra Midi Plus	Macherey-Nagel	Cat#740412.50
Chromium Next GEM Single Cell 5′ Kit v2	10X Genomics	Cat#PN-1000263
Library Construction Kit	10X Genomics	Cat#PN-1000265
HS BRB-seq Library Preparation Kit	Alithea Genomics	Cat#10891
5′ Feature Barcode Kit	10X Genomics	Cat#PN-1000256
Chromium Next GEM Chip K Single Cell Kit	10X Genomics	Cat#PN-1000287
Dual Index Kit TN Set A	10X Genomics	Cat#PN-1000250
DAB chromogen kit	Agilent	Cat#K8000
Permanent Red chromogen	Monosan	Cat#MON-APP185
Mouse IFNγ ELISPOT Set	BD Biosciences	Cat#551083; RRID:AB_2868922
Adeno-X™ Adenoviral System 3 (CMV, Green)	Takara	Cat#632267
Deposited data		
Sequence data MOG – and Spike specific B cells	GenBank NCBI	GenBank: PQ879402 – GenBank: PQ879429
Dataset for transcriptome analysis	GEO NCBI	GEO: GSE308213; https://github.com/julien-roux/Kim_Schneider_et_al_B_cells_expressing_EBV_LMP1_paper
Experimental models: Cell lines		
Human rhabdomyosarcoma (RD) cells	ATCC	Cat#CCL-136; RRID:CVCL_1649
TE671-HA-GFP (stable line)	This paper	N/A
TE671-MOG-GFP (stable line)	This paper	N/A
TE671-SARS-CoV-2-mCherry (stable line)	This paper (per Callegari et al.[36])	N/A
TE671-MOG-CD40L	This paper	N/A
TE671-CD40L	This paper	N/A
BHK-G43	This paper (per Hanika et al.[57])	N/A
HEK-293T	ATCC	Cat#CRL-3216; RRID:CVCL_0063
Experimental models: Organisms/strains		
Mouse: BALB/C-GT(ROSA)26sor$^{tm10(LMP1)Rsky/}$J	The Jackson Laboratory	RRID:IMSR_JAX:019120
Mouse: C57BL/6-Tg(TCRA2D2,TCRB2D2)1$^{Kuch/}$J	The Jackson Laboratory	RRID:IMSR_JAX:006912
Mouse: B6.CG-GT(ROSA)26SOR$^{TM14(CAG-TDTOMATO)HZE/J}$	The Jackson Laboratory	RRID:IMSR_JAX: 007914
Mouse: B6.129P2(C)-CD19$^{tm1(CRE)CGN/}$J	The Jackson Laboratory	RRID:IMSR_JAX: 006785
Mouse: B6.C-CD79A$^{tm3(CRE/ERT2)Reth/}$EhobJ	The Jackson Laboratory	RRID:IMSR_JAX: 033026
Mouse: B6.CG-IGH-J$^{tm1a(Igl)}$	Gurumoorthy Krishnamoorthy	N/A
Mouse: B6.129-IGK^{Flubi}IGH^{Flubi}/HPL	Stephanie Dougan	N/A
Mouse: B6-IGH-J$^{tm1(VDJ-VI10)Zbz}$ x B6-TG(VI10L)^{Ctmb}	Daniel Pinschewer, University of Basel	N/A
Mouse: C57BL/6NCrl	Animal Facility, University of Basel, Charles River	N/A
Mouse: BALB/cJRj	Animal Facility, University of Basel, Janvier Labs	N/A
Mouse: B6-Tg(H2KVa4Vb2)^{213Zbz}	Daniel Pinschewer, University of Basel	N/A
Mouse: C57BL/6-Tg(UBC-GFP)^{30Scha}/J	Radek Skoda, University of Basel	RRID:IMSR_JAX:004353

(*Continued on next page*)

Continued

REAGENT or RESOURCE	SOURCE	IDENTIFIER
Mouse: B6.Cg-Tg(TcraTcrb)^{425Cbn}/J	The Jackson Laboratory	RRID:IMSR_JAX:004194
Mouse: FVB/NRj	Animal Facility,University of Basel, The Jackson Laboratory	RRID:IMSR_JAX:001800
Mouse: CSF1R fl/fl	Deniz Kaymak, University of Basel	N/A
Mouse: Cx3cr1-cREert2-eYFP	Deniz Kaymak, University of Basel	N/A
Recombinant DNA		
vPigLIC	This paper	N/A
pCMV2-HA	Sino Biological	Cat#VG11692-CY
pUltra	Lou et al.[58]	Addgene Plasmid #24129
pEFGP-VSVG	Presley et al.[59]	Addgene Plasmid #11912
pRSV-MOG	Plasmid from Edgar Meinl, Ludwig Maximilian University, Munich)	N/A
pcDNA6.2C-EmGFP-DEST	Invitrogen	Cat#V35520
pcDNA6	Invitrogen	Cat#V22120
pcDNA mCherry LIC cloning vector (6B)	Plasmid from Scott Gradia	Addgene Plasmid #30125
5′-PTK-3′	Plasmid from Alan Bradley, Sanger Institute	N/A
Software and algorithms		
FiJi (ImageJ)	Schindelin et al.[60]	https://imagej.net/software/fiji/; RRID:SCR_003070
Imaris	Oxford Instruments	http://www.bitplane.com/imaris/imaris; RRID:SCR_007370
QuPath	Bankhead et al.[61]	https://qupath.github.io; RRID:SCR_018257
FlowJo (Version 10.10)	BD Life Sciences	https://www.flowjo.com/flowjo/overview; RRID:SCR_008520
Prism (Version 10.2.3)	GraphPad Software, LLC	https://www.graphpad.com; RRID:SCR_002798
R software (Version 4.3.1)	R Core Team (2021)[62]	https://www.R-project.org/; RRID:SCR_001905
Nikon NIS-Elements	Nikon Instruments	https://www.nikoninstruments.com/Products/Software, RRID:SCR_014329
STARsolo (Version 2.7.10a)	Dobin et al.[63]	RRID:SCR_021542
DropletUtils (Version 1.22)	Bioconductor	https://bioconductor.org/packages/release/bioc/html/DropletUtils.html; RRID:SCR_026136
scran (Version 1.30)	Bioconductor	https://bioconductor.org/packages/release/bioc/html/scran.html; RRID:SCR_016944
scater (Version 1.30.1)	Bioconductor	https://bioconductor.org/packages/release/bioc/html/scater.html; RRID:SCR_015954
batchelor (fastMNN – Version 1.18.1)	Bioconductor	https://bioconductor.org/packages/release/bioc/html/batchelor.html; RRID:SCR_017351
SingleR (Version 2.4.1)	Bioconductor	https://www.bioconductor.org/packages/release/bioc/html/SingleR.html; RRID:SCR_023120
celldex (Version 1.12.0)	Bioconductor	https://bioconductor.org/packages/release/data/experiment/html/celldex.html
edgeR (Version 4.0.9)	Bioconductor	https://bioconductor.org/packages/release/bioc/html/edgeR.html; RRID:SCR_012802
limma (voom – Version 3.58.1)	Bioconductor	https://bioconductor.org/packages/release/bioc/html/limma.html
umap (R package)	CRAN	https://cran.r-project.org/web/packages/umap/vignettes/umap.html
FlowSOM (R package)	Bioconductor	https://bioconductor.org/packages/release/bioc/html/FlowSOM.html
FastQC (Version 0.11.9)	Babraham Bioinformatics	https://www.bioinformatics.babraham.ac.uk/projects/fastqc/; RRID:SCR_014583

(*Continued on next page*)

Continued

REAGENT or RESOURCE	SOURCE	IDENTIFIER
Rsubread package (Version 2.0.6)	Bioconductor	https://bioconductor.org/packages/release/bioc/html/Rsubread.html; RRID:SCR_016945
scDblFinder (Version 1.16.0)	Bioconductor	https://bioconductor.org/packages/release/bioc/html/scDblFinder.html; RRID:SCR_022700
Other		
Attane Isoflurane ad us. Vet.	Piramal Pharma	Cat#AP/DRUGS/220/96
Esconarkon ad us. Vet.	Streuli Tiergesundheit AG	Cat#FS04761/004.1
Metacam 5 mg/ml ad us. Vet.	Boehringer Ingelheim	Cat#P20809A-07
Lidocain 2%	Streuli Pharma	Cat#AE16005/000.0
Bupivacain 5 mg/ml	Sintetica	Cat#6811006
Bupaq P ad us. Vet.	Streuli Pharma	Cat#0102301462
Rimadyl ad us. Vet. Carprofenum	Zoetis Schweiz GmbH	Cat#40039886
Betadine	Mundi pharma	Cat#14670-1805
Lacrinorm Carbomerum	Bausch + Lomb	Cat#48038T574
Dafilon 5/0 DS19	B. Braun	Cat#C0932191

EXPERIMENTAL MODEL AND STUDY PARTICIPANT DETAILS

Human Donors

Healthy donors recruited from the staff of the University Hospital Basel gave informed consent and donated 50 ml of blood. Studies involving humans were authorized by the Ethical Committee of Northwest Switzerland (EKNZ project ID 2021-00961). Studies of brain biopsy tissue samples were conducted in accordance with the Freiburg Ethics Commission. Table S1 presents donor demographic information.

Mice

Mouse lines used in the study are listed in Table S1. WT mice used in this study were C57Bl/6Ncrl mice bred in the animal facility at the Department of Biomedicine of the University of Basel. WT tomato mice were obtained by crossing B6.Cg-Gt(ROSA)$^{26Sortm14(CAG-tdTomato)Hze}$/J (Ai14) with B6.129P2(C)-Cd19^{tm1}(cre)Cgn/J (CD19Cre), both from Jackson. Three mouse lines with antigen-specific BCR were crossed with WT tomato mice to yield mice with tdTomato-expressing, antigen specific B cells.

B6(129)-Igk^{FluBI}Igh^{FluBI}/Hpl (FluBI) is a transnuclear mouse line with BCR specific for hemagglutinin from influenza A/WSN/1933, kindly provided by Stephanie Dougan and Hidde Ploegh at Boston Children's Hospital.

B6-Igh-J$^{tm1(VDJ-VI10)Zbz}$ x B6-Tg(VI10L)C^{tmb} (V10l) has a BCR specific for VSV glycoprotein, and was kindly provided by Daniel Pinschewer at the University of Basel.

The Igh-J^{tm1Aigl} IgH (MOG), also called "Th", is a transgenic line with BCR specific for MOG, kindly provided by Gurumoorthy Krishnamoorthy at Max Plank Institute of Biochemistry.

The MOG line was alternatively crossed with B6.C-Cd79a$^{tm3(cre/ERT2)Reth}$/EhobJ and BALB/c-Gt(ROSA)26Sor$^{tm10(Lmp1)Rsky}$/J and B6.Cg-Gt(ROSA)$^{26Sortm14(CAG-tdTomato)Hze}$/J (Ai14) to yield progeny with tamoxifen-inducible expression of the EBV protein LMP1 together with tdTomato in B cells. Controls were generated by choosing littermates with no MOG BCR allele, or no LMP1.

Two antigen-specific CD4 TCR lines were used.

B6-Tg(H2KVa4Vb2)213Zbz has TCR specific for VSV glycoprotein and was kindly provided by Daniel Pinschewer of the University of Basel.

The 2D2 line C57BL/6-Tg(Tcra2D2,Tcrb2D2)1Kuch/J is a transgenic line expressing T cell receptor (TCR) specific for MOG obtained from Jackson. For one experiment this line was crossed with C57BL/6-Tg(UBC-GFP)30Scha/J, kindly provided by Radek Skoda (University of Basel) to yield mice with constitutively GFP-expressing, MOG-specific T cells.

FVB/NRj mice were obtained originally from Jackson and maintained at the University of Basel.

BALB/cJRj mice were obtained originally from Janvier and maintained at the University of Basel.

Studies involving live animals were reviewed and authorized by the animal research office of the cantonal veterinary department of Basel, and the tri-cantonal Animal Research Commission of Basel and Aargau.

Mice housed at the Department of Biomedicine of the University of Basel were kept in SEALSAFE PLUS GM500 cages of up to 5 animals maintained at temperatures between 21° and 25°C and relative humidity of 55% (±10%). Wood shavings were provided for bedding and ennvironental enrichment in the form of paper, plastic tunnels and paper cups for nesting. Light cycle was 12 hours 12 hours light/dark, and standard laboratory chow (Granovit AG 3436EX) and water ad libitum. Animals were monitored daily for the

length of each experiment. Male and female mice were used without distinction, except in experiments involving neonatal pups, in which case the sex was not known. Animals were assigned to experiments semi-randomly, i.e., without conscious choice, but without formal randomization. The youngest animals used were 3 days postnatal, and the oldest 22 weeks.

mouse line	antigen specificity	cre driver	inducible transgene
inducible transgene, and cre driver lines			
Ai14	-	-	tdTomato
LMP1	-	-	LMP1
CD79a-creERT2	-	CD79a-creERT2	-
CD19-cre	-	CD19-cre	-
Cx3cr1-CreERT2-eYFP	-	Cx3cr1-CreERT2	-
CSF1R fl/fl	-	-	Deletes CSF1R
non transgenic lines			
C57Bl/6Ncrl	-	-	-
BALB/cJRj	-	-	-
FVB/NRj	-	-	-
antigen-specific B cell lines			
MOG	MOG	-	-
MOG tomato	MOG	CD19-cre	tdTomato
FluBl tomato	influenza hemagglutinin	CD19-cre	tdTomato
WT tomato	polyclonal	CD19-cre	tdTomato
MOG tam(tomato)	MOG	CD79a-creERT2	tdTomato
MOG tam(LMP1 tomato)	MOG	CD79a-creERT2	tdTomato and LMP1
WT tam(LMP1 tomato)	polyclonal	CD79a-creERT2	tdTomato and LMP1
V10 tomato	VSV glycoprotein	CD19-cre	tdTomato
antigen-specific CD4 T cell lines			
2D2	MOG	-	-
2D2 GFP	MOG	-	GFP (constitutive)
L7	VSV glycoprotein	-	-
OT-II	OVA_{35-55}	-	-

LMP1 = latent membrane protein 1; WT = wild type; MOG = myelin oligodendrocyte glycoprotein; VSV = vesicular stomatitis virus; GFP = green fluorescence protein

Cell culture and immune cell isolation

TE671 rhabdomyosarcoma cells were purchased from ATCC (LGC, Wesel, Germany, CRL-8805) and cultured in RPMI-10 (RPMI medium with 10 % fetal calf serum, 100 units/ml penicillin and 100 μg/ml streptavidin) in 5 % carbon dioxide at 37 °C.

Transgenic B cells and $CD4^+$ T cells were isolated from the spleens of various transgenic animals using the magnetic separation kits from Miltenyi according to the manufacturer's recommendations (see key resources table). In mice in which the expression of transgenes was dependent on tamoxifen induction of CreERT2, tamoxifen was injected at 100 mg/kg ip in corn oil 3 days before organ harvest.

Plasmids, Viruses and viral vectors

The human CD40L plasmid was purchased expression-ready from Sino Biological. A construct encoding mouse CD40L was synthesized by IDT (geneBlocks) and cloned into vPigLIC by ligation independent cloning. VSV*ΔG, a glycoprotein G-deficient VSV encoding green fluorescent protein (GFP) was described by Hoffmann et al..[55] VSV*ΔG was propagated on the BHK-G43 helper cell line providing the VSV glycoprotein G in trans.[57] In VSV-G*, the glycoprotein G gene was fused at the cytoplasmic terminus to GFP and the virus produced on BHK-G43 cells according to a published procedure.[56] VSV-G* did not efficiently replicate in an autonomous manner, most likely because the GFP fusion interfered with VSV G function. Ad-CD40L adenoviral vector mediating expression of CD40L was made and titered with Adeno-X™ Adenoviral System 3 (Takara) according to the manufacturer's instructions, using the murine CD40L sequence amplified from the plasmid described above. CD40L expression mediated by the various constructs was confirmed in HEK cells using flow cytometry. Influenza A/WSN/1933 (H1N1) is a neurotropic influenza virus strain purchased from ATCC. Viruses were titered by serial dilution on sensitive cells and GFP or CD40L expression (for transducing units of VSV

and Adeno CD40L, respectively), or plaque formation for plaque forming units of influenza virus were quantified. vPigLIC was made by replacing the cloning site of 5'-PTK-3' (a kind gift from Alan Bradley, Sanger Institute)[64] with the LIC cloning site amplified from pcDNA mCherry LIC cloning vector 6B.

Stereotactic injections

For intracerebral injections, animals anaesthetized with 2-5 % isoflurane in O_2. 20 - 50 ul of 0.25 % bupivacaine, 0.5 % lidocaine was injected under the scalp immediately after induction of anaesthesia, and the heads were fixed in a stereotaxic device (Stoelting). Corneas were protected with ophthalmic gel (Lacrinorm). The scalp was disinfected with betadine and incised, and the skull was drilled with a micro drill (Stoelting) to make a small hole (0.2-0.3 mm diameter) at coordinates taken from Franklin and Paxinos (2008). The dura was incised with the point of a hypodermic needle, a 28 gauge needle connected to a 10 μl Hamilton syringe was slowly lowered into the brain to a depth of 0.5 mm below the target, then withdrawn slowly to the target depth, and 1 μl of injectate, according to experiment, was injected at a rate of 0.6 μl/min. The needle was withdrawn slowly, and the scalp sutured. For superficial cortical infections, the same procedure was followed, except that the needle of the Hamilton syringe was replaced with a fine glass pipette, and inserted into the superficial cortex at a shallow angle.

Perisurgical analgesia was achieved with either buprenorphine injected ip at 0.05 mg/kg at 30 minutes before the start of surgery followed by Meloxicam (5 mg/kg) sc immediately after, and again one day after the surgery, or alternatively by adding carprofen to the drinking water from one day before until three days after the surgery.

Mouse brain histology

Mice were perfused with PBS followed by 4 % paraformaldehyde in PBS. The brain was dissected out of the skull and fixed in 4 % paraformaldehyde overnight, then stored in PBS + 0.01% sodium azide. 40 μm sections were cut on a vibratome (Leica VT 1200S) and stored in PBS + 0.01% sodium azide at 4 °C until used. For immunolabeling, after various treatments to increase antigen accessibility (see below) sections were incubated in blocking buffer (PBS with 5 % FCS and 0.3 % triton-X) for 15 minutes, then incubated with primary antibodies diluted in blocking solution on a shaker at room temperature overnight, then washed twice with PBS for 5 minutes, followed by washing with PBS + 0.3 % triton for 30 minutes, and incubated with fluorescently labeled secondary antibodies diluted in blocking solution overnight at room temperature. Fluorescent secondary antibodies were obtained from Jackson. The solution was replaced with 1 mg/ml DAPI in PBS for 5 minutes and washed with PBS + 0.3 % triton for 10 minutes. Sections were mounted with Fluoromount G (SouthernBiotech) and images were acquired with a Nikon A1R confocal microscope or Nikon Crest V3 confocal microscope. with a Nikon Ti2 fluorescence microscope, or an automated fluorescent slide-scanning microscope (Nikon upright Ni). For MOG immunolabeling sections were treated before primary antibody incubation for 20 minutes in pre-warmed citrate buffer (pH 6.0) at 98 °C then cooled to room temperature for 20 minutes and washed in PBS thrice. For MBP, C1q and C3d labeling, sections were immersed in neat pre-cooled ethanol at -20 °C for 10 minutes, then washed thrice in PBS before labeling.

Primary antibodies used for immunofluorescent labeling mouse tissues were as follows: axons – chicken anti-neurofilament, Abcam polyclonal antibody Ab24520; IgM^a- mouse monoclonal (directly conjugated with FITC), BD, 553516; myelin - rat anti-bovine MBP, chemicon MAB386, or rabbit anti-human MOG, Cell Signaling,

$CD45^+$ cell retrieval from mouse brains

Mice were perfused with PBS followed by MEM-Hepes with Liberase 0.399 units/ml (Roche) and DNase I 0.2 mg/ml (Sigma-Aldrich) (liberase buffer). Brain, cervical lymph node (CLN), inguinal lymph node (ILN) and spleen (Spl) were harvested. Brain tissue was minced and digested with 3 ml of liberase buffer for 30 minutes in a 37 °C water bath. PBS containing 2 % fetal calf serum and 2 mM EDTA was used for washing and further processing. Digested tissue was mashed through a 70 μm cell strainer (Falcon) then CD45-positive cells were isolated with CD45 microbeads (Miltenyi Biotec), labeled with antibodies after or without fixation with 4 % PFA and permeabilization with 0.1 % saponin for detection in a BD LSRFortessaTM Cell Analyzer or CytoFLEX Flow Cytometer (Beckman Coulter). For scTranscriptomics and ELISpot analysis, tdTomato-positive cells were sorted using BD FACSAriaTM III or BD FACSMelodyTM.

#96457; neurons - rabbit anti-NeuN, Cell Signaling, D353I; astrocytes - rabbit anti-GFAP, Cell Signaling, E4L7M; blood vessel basement membranes - rabbit anti-laminin, Abcam, Ab11575; influenza infected cells - rabbit anti-HA, Sino Biological, 11692. Microglia were labeled with biotinylated *Lycopersicon esculentum* lectin and visualized with fluorophore-conjugated streptavidin (Jackson).

METHOD DETAILS

Mouse tissue resident B cells

Mice were given anti-CD45 (8 μl in 200 μl PBS) iv 5 minutes prior to perfusion. Spleens and lymph nodes were crushed in RPMI-10 in plate wells using syringe plungers. To separate splenocytes from residual tissue fragments, medium containing the immune cells was centrifuged at 300 g for 5 min at 4 °C, the supernatant was discarded, and the pellet was resuspended in 10 ml isolation buffer (PBS + 2% v/v FCS and 5 mM EDTA). The cells were isolated by density gradient centrifugation as described below. Blood was taken from right auricle immediately before perfusion.

Lungs were separated from the right and left main bronchi, which were always processed together with the trachea. Mediastinal lymph nodes (MLN) were dissected with the help of magnifying glasses. Samples of the small intestine and colon were 2 cm long. In the small intestine, samples were taken 1 cm distal of the pyloric sphincter, in the colon after the caecum. Heart samples consisted only of the apical parts of the left and right ventricles. The liver, was dissected as a whole organ without connected vessels, the kidney in addition without the renal pelvis.

Organs were washed with PBS and surrounding connective tissue was removed. Organs were minced with a blade and digested in collagenase buffer (3 ml HBSS + 3 ml PBS + 75 mg Collagenase IV + 412.5 µl DNAse I + 500 µl 1M HEPES) by incubating the samples for 20 minutes in a 37 °C water bath and 20 minutes in a 37 °C, 200 rpm shaking incubator (Kühner Shaker LT-X). Digestion was stopped by adding cold isolation buffer and placing the samples on ice. The suspension was taken for further processing without the remaining solid parts, spun, resuspended again in isolation buffer and filtered using a 70 µl strainer, before isolation of the lymphocytes.

Lymphocytes were isolated from the tissue suspensions by density gradient separation using Percoll. The cell pellet was resuspended in 2 ml 30 % v/v Percoll (30 % v/v SIP + 70 % v/v RPMI). SIP consists of 90 % v/v Percoll + 10 % v/v 10 x PBS. This suspension was slowly layered over 2 ml 70 % v/v Percoll (70 % v/v SIP + 30 % v/v RPMI), then centrifuged at 500 g for 15 min. The interphase was transferred to another flow tube and the cells were washed in 2 ml isolation buffer, centrifuged at 500 g for 5 min, washed again, and kept on ice until staining. After isolation, the cells were blocked with Fc receptor blocker (FCR block, purified anti-CD16/CD32) at a dilution of 1/1000. Afterwards, the cells were incubated for 30 minutes in PBS with AF700 anti-CD3ε, BV510 anti-CD19, BV421 anti-CD20, BV711 anti-CD45R/B220, APC-Cy7 anti-F4/80, AF488 anti-IgM, PE/Dazzle 594 anti-CD138 and PerCP-Cy5.5 anti-CD45.2, using anti-IgM AF488 at a dilution of 1/1000, all other antibodies 1/100. After staining, the cells were washed in isolation buffer and the samples were run on a BD LSRFortessa X-20 cell analyzer.

To analyze the resulting data, dead cells, doublets and CD45-negative cells were excluded via manual gating using FlowJo. Cytometry data were reduced to two dimensions by applying Uniform Manifold Approximation and Projection (UMAP) (“umap” R package, Konopka, 2023).[65] Clustering was performed using the FlowSOM algorithm (“FlowSOM” R package, Van Gassen et al.[66]). Cells were subsequently manually annotated into different clusters based on the normalized median fluorescence intensity of selected markers.

In vitro live cell imaging

To image capture of influenza hemagglutinin (HA) by HA-specific B cells, TE cells were seeded in 8 well chambered coverslips (Ibidi #80826) and the next day, at 60 - 80 % confluence, transfected with pUltra WSN-HA-GFP using JetPrime. The following day, the chamber was transferred to a temperature and CO2 controlled chamber on the stage of a Nikon Ti2 Deep Thought spinning disk confocal microscope. Every two minutes, for one hour, 5-plane stacks of images were collected in the brightfield, GFP, and AlexaFluor 647 channels with a 60x Plan Apo Lambda D oil immersion objective lens. After six minutes, splenocytes from a FluBI mouse were added, with the B cells labeled with rat anti-mouse CD19 AlexaFluor 647 (BioLegend 115522). Acquisition was controlled by Nikon Images software, and processed with ImageJ (Fiji).

In vitro antigen capture assay

TE671 rhabdomyosarcoma cells were cultured in RPMI R-10 in an incubator with 5 % carbon dioxide at 37 °C. Stably HA-transfected cell lines (TE HA-GFP) were made by transfecting TE 671 cells with vPigLIC HA-GFP encoding GFP-fused hemagglutinin from influenza A/WSN/1933. Transfected cells were selected and maintained in R-10 with 0.25 µg/ml of puromycin. For the capture assay, these cells were seeded in 12-well-plates, and when 90% confluent, B cells from FluBI or wild type mice were added. At 0, 15, 30, 60, 120, 240 minutes B cells were retrieved with 2 ml of ice-cold PBS, labeled with goat anti-mouse immunoglobulin (Jackson 115-605-003), washed and acquired on a Cytoflex flow cytometer. Each data point included at least 5000 cells from one co-culture well, results pooled from three independent experiments, each with three co-culture wells per time point.

B cell lung infiltration and antigen capture

For intranasal influenza infections, C57Bl/6 mice were lightly anaesthetized with vaporized isoflurane (2-3 % in O_2), and held by the scruff of the neck in a vertical position with the snout uppermost. 50 µl of PBS containing 20,000 infectious units of influenza A/WSN/1933 was pipetted onto each nare, and the mouse was allowed to inhale it before being returned to the cage. Three days later, a mixture of 2.5 million CTV-labeled FluBI tomato and the same number of unlabeled WT tomato B cells were adoptively transferred iv, and then the mice were sacrificed one or three hours later.

For histological investigations, mice were transcardially perfused with PBS and 4 % paraformaldehyde in PBS, lungs were dissected out, embedded in 4 % w/v TopVision low melting point agarose gel at 40 °C, and incubated on ice for 15 minutes. The samples in gel blocks were glued to the stage and sectioned on a Leica VT1200S at 200 - 300 µm, and immunolabeled as described above in “mouse brain histology”. At least 30 images like the one shown in Figure 1F were captured for each mouse (WT tomato, n =4; FluBI tomato, n=3) and scored by a blinded investigator on a scale of 0 (no interaction) to 5 (most intimate interaction) as shown in Figure S1E.

Membrane antigen capture RNA-seq

B cells from MOG tomato mice were isolated and cocultured with TE671 cells or with TE671 rat MOG or without feeder cells but in the presence of 5 μM F(ab′)2 donkey anti-mouse IgM cells for 4 hours, before retrieval and lysis and RNA extraction with the Quick-RNA MicroPrep kit Zymo, Cat R1051, according to the manufacturer's instructions. Library preparation was performed starting with 30 ng of total RNA of each sample using the HS BRB-seq Library Preparation Kit (Cat. #10891; Alithea Genomics, Epalinges, Switzerland). Sequencing was performed on an Illumina NovaSeq 6000 instrument to produce paired-end 51nt reads. Data analysis was performed by the Bioinformatics Core Facility, Department of Biomedicine, University of Basel. Read quality was assessed with the FastQC tool (version 0.11.9). Reads were mapped to the hybrid reference comprising human and mouse genomes (hg38 and mm10) with STAR (version 2.7.10a) with default parameters, except filtering out multimapping reads (outFilterMultimapNmax=1) and filtering reads without evidence in the spliced junction table (outFilterType=''BySJout''). The featureCounts function from the Rsubread package (version 2.0.6) was used to count the number of reads (5' ends) overlapping with the exons of each mouse gene (Ensembl release 102) assuming an exon union model. Subsequent analyses were performed using the R software (version 4.3.1) and Bioconductor 3.18 packages. CPM values were calculated, log-transformed and normalized with a cyclic-loess normalization using the normalizeBetweenArrays() function from the limma package. A total of 9,071 genes with logCPM above 4 in at least 3 samples (n-1 the number of biological replicates) were retained for the the next steps. A principal component analysis (PCA) was performed on the top 500 genes with highest inter-quartile range using the prcomp() function. For

To account for complexity differences commonly observed in RNA-seq libraries, the function voomWithQualityWeights() from the limma package (version 3.58.1) was used (with a cyclic loess normalization) to combine observational-level with sample-specific quality weights prior to differential expression analysis comparing MOG or IgM-stimulation to unstimulated conditions. P-values were adjusted by controlling the false discovery rate (FDR; Benjamini-Hochberg method) and genes with a FDR lower than 5% were considered significant.

An activation signature of 124 genes was obtained by selecting genes differentially expressed at an FDR of 15 and with a log2 Fold-change above 2, between MOG-stimulated and unstimulated conditions.

Brain VSV infections and B cell infiltration

WT tomato mice were injected stereotactically with 5000 transducing units of VSV*ΔG at coordinates 0.5 mm rostral from bregma, 2 mm left of center, 2.5 mm ventral to dura, as described above. 2, 5, or 7 days later, mice were perfused and brains processed for immunofluorescent histology as described above. Oligodendrocytes were labeled with rat anti-bovine MBP, Chemicon MAB386, neurons with rabbit anti-NeuN, Cell Signaling, D353I; astrocytes - rabbit anti-GFAP, Cell Signaling, E4L7M; blood vessel basement membranes - rabbit anti-laminin, Abcam, Ab11575. Microglia with biotinylated *Lycopersicon esculentum* lectin and visualized with fluorophore-conjugated streptavidin (Jackson). B cells were visualized with the endogenously encoded tdTomato, and were counted in the parenchyma or in the laminin-labeled perivascular spaces by an observer blinded to the experimental groups.

In vitro VSV capture live cell imaging

Mouse primary cortical cells were prepared by triturating the telencephalon of neonatal mouse pups and culturing the cell suspension in DMEM with 10% FCS for one week. Cells were then trypsinized and transferred to an 8-well chambered coverslip (Ibidi #80826), and allowed to adhere for two days before infection with VSV-G*.

The next day, B cells were extracted from splenocytes and inguinal lymph node cells from V10 or WT mice using Pan B cell Isolation Kit II, mouse (Miltenyi Biotec 130-104-443) and added to the infected cortical cells. *In vitro* live cell imaging was acquired in a humidified 5 % carbon dioxide chamber at 37 °C with a Nikon Ti2 fluorescence microscope with a 40x objective for 0.5-2 hours. Velocities of B cells during antigen capture were extracted using Imaris software. For the V10 tomato B cells, each track was split into before and after antigen encounter.

Intravital imaging

To image the capture of VSV glycoprotein antigen in the cerebral cortex by V10 B cells we infected V10 tomato mice in the striatum by stereotactically injecting 5000 transducing units of VSV*ΔG at coordinates 0.5 mm rostral from bregma, 2 mm left of center, 2.5 mm ventral to dura, to induce B cell infiltration, then 5 days later reinfected them in the superficial cortex with 1000 transducing units of VSV-G*, mediating expression of the VSV glycoprotein that is the target of the V10 B cells (This virus cannot be used to induce B cell infiltration, because it is replication competent and leads to the death of the mice before B cells have had time to infiltrate). Two days after the second infection, we visualized the interaction between tomato-expressing B cells and GFP-G-expressing, virus-infected cells by two-photon microscopy. Mice were anaesthetized with vaporized isoflurane (2% in O_2) and the corneas protected with ophthalmic gel (Lacrinorm). Skulls were exposed by removing the suture made at the time of infection, and fixed with respect to the microscope stage with a custom-made metal bar in a Nikon A1R two-photon microscope. Body temperature was maintained with a heating pad during imaging. The space between the objective lens and the cortex was filled with ophthalmic gel. 200 μm Z-stacks of GFP-expressing infected cells and tdTomato-expressing B cells were recorded for up to one hour. Physiological saline was injected sc to avoid dehydration, and mice were euthanized at the end of the imaging session. B cell extravasation from cortical blood vessels was achieved with the same paradigm, but using MOG tomato mice rather than V10 tomato, in one case with and in one case without the VSV infections.

ELISpot

Interferon-γ production from T cells in response to antigen presentation by B cells was investigated by ELISpot using Mouse interferon-γ, ELISpot kit (BD Biosciences) according to the manufacturer's instructions. 1.6 million 2D2 T cells or 1 million L7 T cells and 4,000 – 8,000 B cells isolated from different mouse organs were seeded and incubated in the capture-antibody-coated ELISpot plate for five days in a humidified carbon dioxide incubator (5 % CO_2 at 37 °C). The resulting spots were counted using an ELISpot reader and analyzed using ImageJ (FIJI). To determine sensitivity and specificity of this assay, we repeated it with MOG or V10 B cells from the spleens of naïve animals, exposed them for 3 hours to TE cells expressing either rat MOG or VSV glycoprotein, then pulsed them or not with $OVA_{323-339}$ peptide (peprotech) at 10 μg/ml for 1 hour at 37 °C, then added them to L7 or 2D2 or OT-II T cells in the ELIspot plate and developed and counted the interferon-γ, spots as above.

Brain-infiltrating B cell IgM^a flow cytometry

CD45+ cells were retrieved from brain as described above, and together with lymph node and spleen cells, were labeled for flow cytometry. To distinguish between genuine MOG-reactive cells and others (in this mouse line variable proportions of peripheral B cells have other immunoglobulin heavy chains than the transgene),[26] we used an antibody specific for the IgM^a allotype, which discriminates the mu constant gene of the background line from the transgenic heavy chain.[67]

scRNAseq brain-infiltrating immune cells

Mice were infected intrastriatally with VSV*ΔG as described above, and in some experiments also with Ad-CD40L. On day 7, 21, or 28 post-injection according to experiment, brains were harvested from perfused mice and tdTomato+, CD45+ cells were labelled with TotalSeq-C anti-mouse Hashtag antibody (1:100, Biolegend 155861, 155863, 155865, 155867, 155869 and 155871). The tdTomato-expressing B cells were then sorted using BD FACSMelody™. scRNA cDNA library was produced using the Chromium Next GEM Single Cell 5' Library kit v2 (Dual Index) (10x Genomics). In each experiment a sample from each condition was used in the pool, with a total of 3 pooled libraries for experiment 1, and 2 pooled libraries for both brain and lymph node for experiment 2. Sequencing libraries were prepared at the Genomics facility using the 10X 5'end v2 kit.

Sequencing was performed on an Illumina NovaSeq 6000 sequencer at the Genomics Facility Basel, ETH Zurich. The dataset was analyzed at the Bioinformatics Core Facility, Department of Biomedicine, University of Basel. STARsolo[63] (version 2.7.10a) was used to perform sample and cell demultiplexing, alignment of reads and UMI counting, with options –outFilterType=BySJout –outFilterMultimapNmax=10 –outSAMmultNmax=1 –outFilterScoreMin=30 –soloCBmatchWLtype=1MM_multi_Nbase_pseudocounts –soloUMIfiltering=MultiGeneUMI_CR –soloUMIdedup=1MM_CR –soloType=CB_UMI_Simple –soloStrand=Reverse –soloUMIlen=10 –soloCellFilter=None –soloMultiMappers=EM. The mouse reference genome mm39 and Ensembl 110 gene models were used, supplemented by construct sequences found in the mouse lines used in both experiments (Neomycin, Cre, tdTomato, Ighv-MOG, Ighv-FluBI and Igkv-FluBI). Endogenous sequences of Ighv1-50 and Igkv4-74, highly similar to the FluBI line constructs Ighv-FluBI and Igkv-FluBI, were masked. Cell hashing barcodes were mapped to a custom reference index including all barcodes used in the experiment, with STARsolo and similar options, except –soloStrand Forward.

Processing of the UMI counts matrix was performed using Bioconductor (version 3.18) packages, notably DropletUtils (version 1.22, function emptyDrops() using 5000 iterations, the option test.ambient=TRUE, a lower threshold of 100 UMIs and an FDR threshold of 0.1%) (Lun et al.[68]), scran (version 1.30) (Vallejos et al.[69]; Lun et al.[70]) and scater (version 1.30.1) (McCarthy et al.[71]), following mostly the steps illustrated in the OSCA book (Amezquita et al.[72]) (http://bioconductor.org/books/3.18/OSCA/). Cells with 0% or more than 4% of UMI counts attributed to mitochondrial genes, with less than 2000 UMI counts, or with less than 1000 detected genes were excluded. The presence of doublet cells was investigated with the scDblFinder package (version 1.16.0) (Germain et al.[73]), and suspicious cells were filtered out using a fixed score threshold of 0.8. HTO demultiplexing was performed with the DropletUtils function hashedDrops(), specifying the relative abundance of each HTO in the ambient solution, and setting doublet_nmads=3, doublet_min=2 and doublet_mixture=FALSE. Cells not assigned to any sample or identified as doublets were filtered out. The package SingleR (version 2.4.1) (Aran et al.[74]) was used for cell-type annotation of the cells using the celldex package (version 1.12.0) and mouse bulk references ImmGenData and MouseRNAseqData. Pruned labels were used, and contaminant cells not annotated as B cells were filtered out. To overlay samples before clustering, the systematic differences between samples were removed using the fastMNN function (k=15) of the batchelor package (version 1.18.1) (Haghverdi et al.[75]). A tSNE embedding for visualization of cells was calculated using the batch-corrected low-dimensional coordinates for cells (perplexity=50). Shared nearest-neighbor graph clustering was performed using the Louvain algorithm for community detection (k=5), resulting in 11 clusters. The scran function scoreMarkers() was used to identify the best cluster markers, based on the mean AUC criterion. Differences in relative abundance of transgenic cells across conditions, or of transgenic cells across clusters were tested using the package edgeR (version 4.0.9) (Chen et al.[76]).

To identify transgenic cells in FluBI or MOG mice samples, an additional STARsolo run was used, with option –outFilterMultimapNmax 1 to consider only uniquely mapping reads mapping to BCR sequences. A cell was considered transgenic in MOG mice samples if no heavy chain gene was expressed at higher level than the transgenic heavy chain construct Ighv-MOG. A cell was considered transgenic in FluBI mice samples if no heavy chain gene was expressed at higher level than the transgenic heavy chain construct Ighv-FluBI and if no light chain gene was expressed at higher level than the transgenic light chain construct Igkv-FluBI.

The gene signature for antigen-induced apoptosis was obtained from Münchhalfen et al.[28] The matrix of mapped read counts was obtained from GEO (GSE237799) and genes significantly down-regulated upon TFEB knock-out in mouse primary germinal center B rcells were extracted using the function voom() from the limma package (version 3.58.1), accounting for the batch structure of the dataset in the design matrix.

In vitro MOG-specific B-T cell interaction

CTV-labeled, MOG-specific B cells were exposed to MOG-expressing TE671 rat MOG cells or control TE671 cells for 3 hours, then retrieved and co-cultured either alone or with 2D2 T cells for 8 days. Flow cytometry was used to enumerate CTV-low, CD19+, B220+ proliferating B cells.

In vivo MOG-specific B-T cell interaction

MOG tomato or WT tomato mice were adoptively transferred with 30 million naïve GFP-expressing 2D2 T cells and then two days later infected intrastriatally with VSV*ΔG as described above. 28 days after infection mice were perfused, and brains sectioned and immunolabeled for MBP as described above. B cells were identified by tdTomato expression and T cells by GFP.

The reverse paradigm used 2D2 mice, or 2D2-non-transgenic littermates infected instriatally, and adoptively transferred 5 days later with 20 million MOG tomato B cells. B cells were visualized with the endogenously encoded tdTomato, and were counted by an observer blinded to the experimental groups. Scoring was done by investigators blinded to experimental groups, following the following system: 0.5 noticeable tail weakness; 1 limp tail; 2 mild hind limb paresis; 2.5 strong hind limb paresis; 3 hind limb hemiplegia; 3.5 bilateral hind limb paralysis; 4 forelimb weakness.

2D2 activation and adoptive transfer

Splenocytes from a 2D2 mouse were cultured for 2 days in the presence of 20 μg/ml MOG_{35-55}, and 5 ng/ml each of IL-2 and IL-7 in RPMI-10 at 37 °C, in 12-well plate wells at 4 million per ml, then diluted to 1 million per ml and incubated for another 4 days in the same medium but without MOG peptide. They were then incubated for 24 hours in RPMI-10 with 20 ng/ml IL-12 and 24 ng/ml IL-18 in a plate pre-coated with anti-CD3 and anti-CD28 at 2 μg/ml. These activated T cells, or naïve equivalents taken from other mice were then washed twice in PBS and adoptively transferred into FluBI or MOG mice at 3 million per mouse, 5 days after intrastriatal infection with VSV*ΔG. Mice were weighed and scored every day, and as soon as the first mouse exceeded a score of 2, all mice were injected intravenously with 5 μg of anti-CD45 in 100 μl total volume PBS 3 minutes before pentobarbital overdose and transcardial perfusion with PBS.

Brains were processed and digested for 30 minutes using the gentleMACS™ Octo Dissociator with Heaters (37C_ABDK_01). Samples were incubated for 10 minutes at 37 °C on a shaker. Samples were then homogenized through an 18-gauge needle and filtered through a 100 μm cell strainer. The single cell suspension was resuspended in 30 % (v/v) Percoll followed by gradient centrifugation at 1350 g for 30 minutes with no break at 4 °C. The uppermost layer containing myelin was removed, and cells from the pellet washed and divided into two, one half was immediately labeled with antibodies for flow cytometry, and the other half was restimulated for 4 hours at 37 °C in RPMI containing 50 ng/ml phorbol myristate acetate, 500 ng/ml ionomycin, 1x Brefeldin A and 1x monensin. Cells were then washed and fluorescently labeled for flow cytometry.

Fluorescently labeled antibodies staining of cell surface antigens was performed for 30 minutes at 4 °C. Samples were then washed and fixed for 30 minutes at 4 °C using True-Nuclear™ Transcription Factor Buffer Set. Fixed samples were washed with 1x Permeabilization Buffer. Intracellular cell staining with fluorescently labelled antibodies was performed overnight at 4 °C. After staining, the samples were washed with permeabilization buffer and PBS before acquiring them on the Cytek® Aurora Spectral Analyzer (Cytek® Biosciences).

To analyze the resulting data, dead cells, doublets and CD45-negative cells were excluded via manual gating using FlowJo. Cytometry data were reduced to two dimensions by applying Uniform Manifold Approximation and Projection (UMAP) (“umap” R package, Konopka, 2023[65]). Clustering was performed using the FlowSOM algorithm (“FlowSOM” R package, Van Gassen et al.[66]). Cells were subsequently manually annotated into different clusters based on the normalized median fluorescence intensity of selected markers.

CD40L and B cell proliferation *in vitro*

CTV-labeled B cells from MOG mice were co-cultured with TE671 or TE671 rat MOG either transfected or not with mouse CD40L, in the presence or absence of naïve 2D2 T cells for 3 days. Proliferating B cells CTV-low, B220+, CD19+ were enumerated by flow cytometry.

CD40L administration *in vivo*

MOG tomato and WT tomato mice were infected intrastriatally with VSV*ΔG as described above, in some cases with co-administration of 3×10^7 transducing units of Adeno CD40L. 28 days later, mice were perfused and sections of brain immunolabled for MOG and IgM^a. The medial dorsal area of the striatum was taken as the region of interest, and myelin segmented and quantified according to

MOG signal below an empirically determined threshold, were extracted automatically using QuPath software, as shown in Figure S5E. Numbers of tdTomato-expressing B cells in the brain tissue were quantified using Qupath according to tdTomato signal above an empirically determined threshold.

This series of experiments was then repeated and instead of fixing and sectioning the brains for histology, mice were perfused with PBS and CD45+ cells retrieved for scRNAseq as described above.

LMP1 and B cell proliferation *in vitro*

CTV-labeled B cells from tamoxifen-treated MOG tam(tomato) or MOG tam(LMP1 tomato) mice were exposed to TE671 rat MOG or TE671 cells for 3 hours, then retrieved and co-cultured either alone or with 2D2 T cells for 6 days. Cells were then retrieved and labeled for IgM^a and CD19. Proliferating B cells (tdTomato+, CTV-low) were enumerated by flow cytometry.

RNA-seq LMP1 versus CD40L

B cells from tamoxifen-treated MOG tam(tomato) or MOG tam(LMP1 tomato) mice were isolated and cocultured with TE671 rat MOG or TE671 cells for 3 hours, then retrieved and cultured with for 4 hours with TE671 CD40L or TE671 cells before retrieval and lysis and RNA extraction with the Quick-RNA MicroPrep kit Zymo, Cat R1051, according to the manufacturer's instructions. Library preparation was performed starting with 30 ng of total RNA of each sample using the HS BRB-seq Library Preparation Kit (Cat. #10891; Alithea Genomics, Epalinges, Switzerland). Subsequently, 14 ng of cDNA was used for tagmentation. An additional PCR (5 cycles) was carried out following the BRB-seq protocol, employing the Equinox Library Amplification Kit (Cat. #7K0014-096; Watchmaker Genomics, Boulder, CO, USA).

Final libraries were sequenced on an AVITI platform (Element Biosciences, San Diego, CA, USA) with the AVITI 2×75 Sequencing Kit Cloudbreak FS High Output (Cat. #860-00015) in paired-end mode (29 bp read 1 / 121 bp read 2), applying a PMG shift of 2 during run setup. STARsolo [77] (version 2.7.10a) was used to perform sample demultiplexing, alignment of reads and UMI counting, with options --soloUMIdedup=1MM_Directional –soloUMIfiltering=”-“ –soloCBmatchWLtype=1MM –outSAMmapqUnique=60 –quantMode=GeneCounts –soloType=CB_UMI_Simple –soloCBstart=1 –soloCBlen=14 –soloUMIstart=15 –soloUMIlen=14 –soloBarcodeReadLength=0 –outFilterMultimapNmax=1 –soloStrand=Forward –soloMultiMappers=Unique. A hybrid reference comprising human and mouse genomes (hg38 and mm39), supplemented by construct sequences Cre, tdTomato, Ighv-MOG and LMP1 (https://www.ncbi.nlm.nih.gov/gene/3783750) was created and the mouse gene models from Ensembl release 110 were used. The sample barcode whitelist Set D was used.

Quality control and differential expression analysis was performed as described above on the 10,136 protein-coding genes with logCPM above 4 in at least 2 samples (n-1 the number of biological replicates). The Xist and Y-chromosome genes were excluded because some conditions in the experiment were partially confounded with sex, a factor which was not of main interest for this study.

Ex-vivo organotypic slice culture

Cerebellar slice cultures were prepared as previously described[77] from 9 day-old FVB mouse pups. The cerebellum was dissected in ice-cold preparation medium (MEM, 1 % Glutamax (Invitrogen), pH 7.3), cut sagittally into 350 μm slices on a McIllwain tissue chopper. Slices were separated, transferred and cultured on permeable membranes (Millicell-CM, Millipore) in sterile neurobasal medium in a humidified atmosphere with 5 % CO2 at 37 °C. B cells were isolated from tamoxifen-treated MOG tam(LMP1 tomato) and MOG tam(tomato) mouse spleens and added on top of the cerebellum slices in culture on the same day. B cells were co-cultured with the cerebellum slices for 7 days, medium was changed every 2-3 days. Cultures were fixed overnight in 4 % PFA in PBS and immunolabeled. Permeable membranes, containing the fixed cerebellum slices and cells, were washed in PBS and incubated in ice-cold ethanol at -20 °C for 10 minutes. Slices were washed in PBS, blocked with 5 % Normal goat serum (NGS), 0.3 % tritonX for 20 minutes at room temperature then incubated with primary antibodies in blocking solution for 72 hours: chicken anti-MBP (1:400) (Invitrogen, PA1 10008) and rabbit anti-NEFL (1:200) (Invitrogen, MA5-14981). Slices were washed with PBS and incubated with secondary antibodies in blocking solution for 72 hours: DAPI, goat anti-chicken Alexa Fluor® 647, goat anti-rabbit Alexa Fluor® 488 (Jackson Immuno, 111-545-144) and goat anti-mouse Rhodamine Red™-X AffiniPure™ (Jackson Immuno, 115-295-166). Slices were then washed in PBS, gently lifted from the membranes and mounted with Fluoromount-G. Mounted slices were imaged using Nikon Crest V3 spinning disk confocal microscope. We investigated the role of microglia in the observed demyelination with two paradigms. Firstly, we repeated the same experiment, but immediately after slice preparation, added to the culture medium at 2 or 20 μM to deplete the microglia, and maintained at this concentration for the 1-week culture period. Control slices received an equal volume of DMSO vehicle. Alternatively, we used pups from the mouse crosses CX3CR1 Cre/wt x CSF1R fl/fl, in which tamoxifen administration mediates depletion of microglia, and CX3CR1 Cre/wt x CSF1R wt/wt as a control. In this paradigm, 4-hydroxytamoxifen was added to the culture medium at 1 μM immediately after slice preparation and maintained for the 1-week duration of the culture. Slices were then immunolabeled as above, with the addition of rabbit anti-IBA1 at 1:1500 to label the microglia and confirm their depletion.

MOG-reactive, LMP1-expressing B cells *in vivo*

MOG tam(tomato), MOG tam(LMP1 tomato), or WT tam(LMP1 tomato) mice were injected intrastriatally with VSV*ΔG, and then 2 days later with tamoxifen-induced B cells from littermates. This resulted in a transfer of B cells from pure C57BL/6 B background

to mice of the same background MOG tam(tomato), or transfer of B cells with a mixed C57BL/6 x Balb/c background to recipients also with a mixed background MOG tam(LMP1 tomato) and WT tam(LMP1 tomato). Twelve days later, recipient mice were sacrificed by perfusion fixation, and brains sectioned and immunolabeled for neurofilament and myelin. Areas from each section that contained normal-appearing axons as shown by NFL, but depleted of myelin, determined as MOG signal below an empirically determined threshold, were extracted automatically using QuPath software from a region of interest including the dorsal striatum and corpus callosum, as shown in Figure S6D. Numbers of tdTomato-expressing B cells in the brain tissue were quantified using Qupath. Two series of sections from the same mice were labeled in parallel for C1q and for C3d, and the area of labeling of each was quantified using Fiji.

Limb use asymmetry testing

2D2 mice (F1 hybrids of 2D2 on C57BL/6 background with WT Balb/c) were injected stereotactically with VSV*ΔG (0.6 mm caudal of bregma, 2 mm left, 4 mm ventral of dura) and three days later were injected stereotactically at the same coordinates with 100,000 tamoxifen-induced B cells from MOG tam(tomato) or MOG tam(LMP1 tomato) mice. At days 0, 5, 8, 11, 16, and 21, limb use was assessed in a video recorded rearing task paradigm (Cylinder test[34]). Mice were placed in the dark for 15 minutes, then placed one at a time into a 5-liter glass cylinder screened from outside with a box. Their movements were recorded from above for 3 minutes per mouse and the videos subsequently scored by a blinded investigator to quantify the number of paw placements on the wall of the cylinder with each forelimb. Limb use asymmetry was calculated for each time point as ipsilateral paw placements (touching the wall of the cylinder with the forepaw ipsilateral to the injected hemisphere) minus contralateral paw placements, and each measurement was corrected for the baseline asymmetry of the individual animal. Two cohorts of animals were sacrificed for flow cytometry of brain immune cells at day 16 and day 21 after virus injection by pentobarbital overdose and transcardial perfusion with PBS.

Brains were processed and digested for 30 minutes using the gentleMACS™ Octo Dissociator with Heaters (37C_ABDK_01). Samples were incubated for 10 minutes at 37 °C on a shaker. Samples were then homogenized through an 18-gauge needle and filtered through a 100 μm cell strainer. The single cell suspension was resuspended in 30 % (v/v) Percoll followed by gradient centrifugation at 1350 g for 30 minutes with no break at 4 °C. The uppermost layer containing myelin was removed, and cells from the pellet washed and labeled with fluorescently labeled antibodies against surface antigens for 30 minutes at 4 °C. Samples were then washed and fixed for 30 minutes at 4 °C using True-Nuclear™ Transcription Factor Buffer Set. Fixed samples were washed with 1x Permeabilization Buffer and intracellular cell staining was performed overnight at 4 °C. After staining, the samples were washed with permeabilization buffer and PBS before acquiring them on the Cytek® Aurora Spectral Analyzer.

To analyze the resulting data, dead cells, doublets and CD45-negative cells were excluded via manual gating using FlowJo, and populations of interest gated manually.

Human antigen-specific cell sorting by MACACS

The procedure for sorting MOG- and SARS-CoV-2-specific B cells followed closely the method described by Callegari et al.[36] Peripheral blood mononuclear cells (PBMC) were separated from human venous blood by density gradient centrifugation, and B cells isolated using the Pan B cell isolation kit, human (no. 130-101-638, Miltenyi). B cells were added to a monolayer of adherent, CTV-labeled TE671 cells stably transfected with MOG-GFP (plasmid encoding full-length human MOG fused to GFP was a kind gift from Edgar Meinl, Ludwig Maximilian University, Munich) and allowed to bind for 20 minutes before gently washing off the non-bound B cells and adding these to a similar layer of TE671 cells stably expressing SARS-CoV-2 fused to mCherry, and after an additional three hours of culture, B cells were stringently washed off both cell layers, labeled with brilliant violet 785-conjugated anti-human CD69 and the antigen-capturing (i.e., GFP- or mCherry-high), CD69-high B cells sorted. Single B cells were seeded at approximately 0.75 cells/well in 384-well plates containing 75 ml of RPMI, 40 % FCS, with 5,000 irradiated TE-CD40L cells and 3.75 ng human IL-21 per well and cultured for 9 days before measuring antibody specificity in the supernatant using the flow cytometric method shown in Figure 1A. From some positive wells, RNA was extracted from the cell lysate using the Zymo quick-RNA kit (R1050), reverse transcribed with reverse transcribed with the SMART-Seq v4 Ultra Low Input RNA Kit for Sequencing (Takara, 634888) and used to prepare sequencing libraries with the DNA prep kit (Illumina). One million, 150 base, paired-end 150 bp reads were to immunoglobulin gene sequences were extracted from the resulting single-cell transcriptomes with a custom script in R and assembled with CAP3. Somatic hypermutation was assessed with the IgBlast tool from ncbi.

LMP1 expression in MS lesions

We assessed tissues from 6 individuals diagnosed with MS, 3 samples from individuals with EBV-associated neoplastic disorders and 3 individuals with no CNS immune-mediated disorder. Human formalin-fixed paraffin-embedded tissues from biopsies and autopsies were cut into 3 μm sections. Antigen retrieval was conducted at pH 9. For immunohistochemistry, samples were sequentially incubated with anti-LMP1 (Santa Cruz Biotechnology sc-71023, 1:200) and anti-CD20 (Dako IR604, ready-to-use) antibodies. We visualized antibody binding using chromogen staining with DAB (Dako K8000, for LMP1 reactions) and Permanent Red (Monosan MON-APP185, for CD20 reactions). Representative images were taken on an Olympus BX41 brightfield microscope. For immunofluorescence labelling, samples were labelled with anti-LMP1 (Santa Cruz Biotechnology sc-71023, 1:200) and anti-CD20 (Cell Signaling E3N70, 1:200) antibodies and respective secondary anti-rabbit/anti-mouse antibodies (Thermofisher, A11004 & A21208). Representative fluorescence images were taken on a Keyence BZ-X810 microscope.

QUANTIFICATION AND STATISTICAL ANALYSIS

Quantitative data were assessed for normality and if suitably distributed were analyzed by two-tailed t-test for two groups, and for three or more groups by one-way or two-way analysis of variance (ANOVA) with appropriate post-hoc tests, as specified in the figure legends. Data that deviated from normality according to the Kolmogorov-Smirnoff test were instead analyzed with appropriate non-parametric tests. Bar charts show means and standard deviations.

CellPress
OPEN ACCESS

Supplemental figures

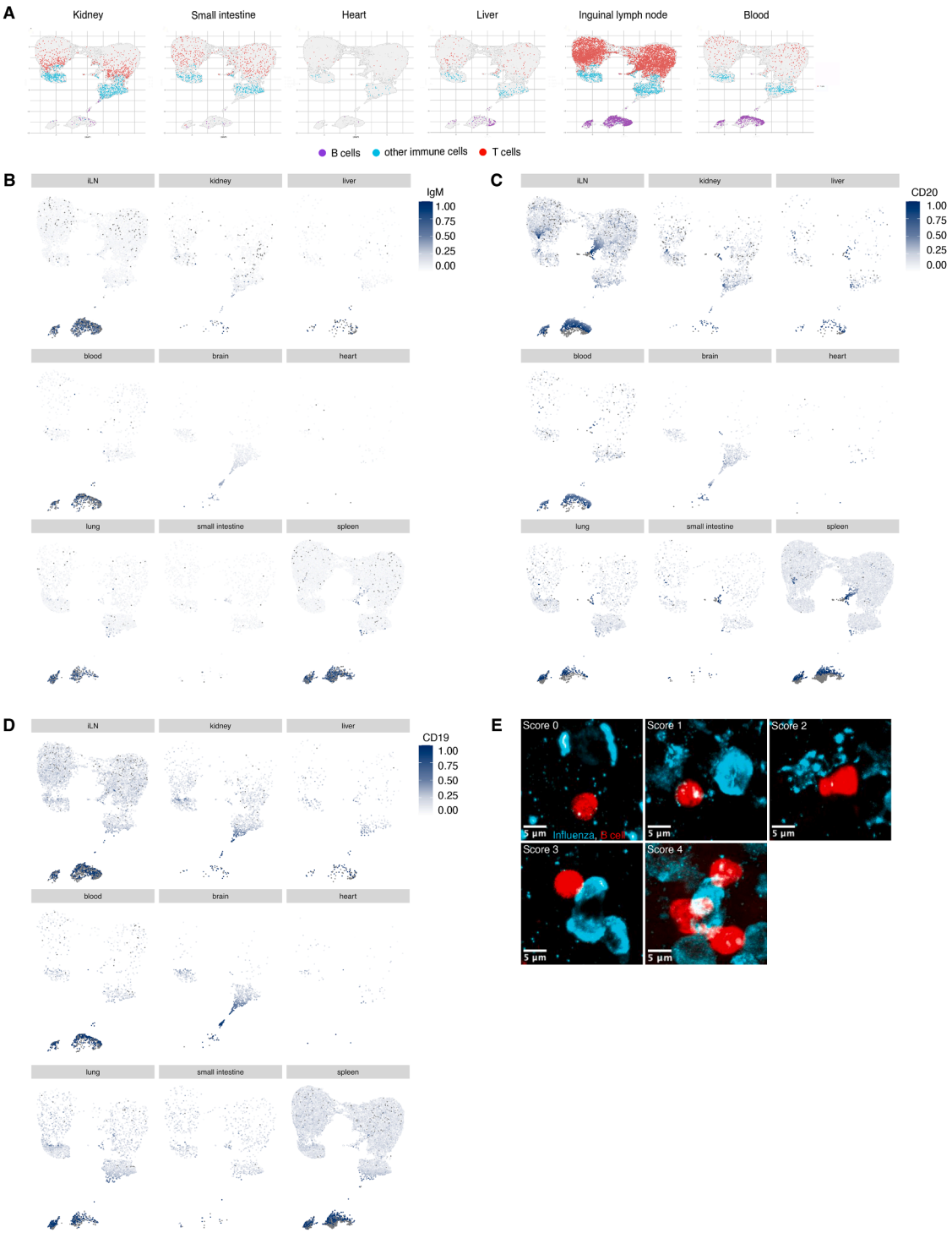

(legend on next page)

Figure S1. Tissue surveillance and membrane antigen capture by B cells, related to Figure 1

(A) UMAP of immune cells from various tissues, colored to show clusters of phenotypically similar cells, as shown in Figure 1A. WT tomato mice were given intravenous anti-CD45 to label intravascular cells, then immediately sacrificed, organs dissociated, and immune cells labeled for flow cytometry with markers of B cells, T cells, and other immune cells, such as macrophages and natural killer (NK) cells (see key resources table).

(B–D) UMAPs of B cells from various tissues, as shown in Figure 1A, colored according to the expression of the specified marker. (B) IgM. (C) CD20. (D) CD19.

(E) Representative confocal images scored for intimacy of contact between infiltrating B cells (red) and influenza-infected lung parenchymal cells (cyan), used to derive the scores shown in Figure 1G. Score 0 (top left image) indicates no obvious contact, whereas score 5 (shown in Figure 1F) indicates direct contact over more than half of the B cell surface. See also Video S2.

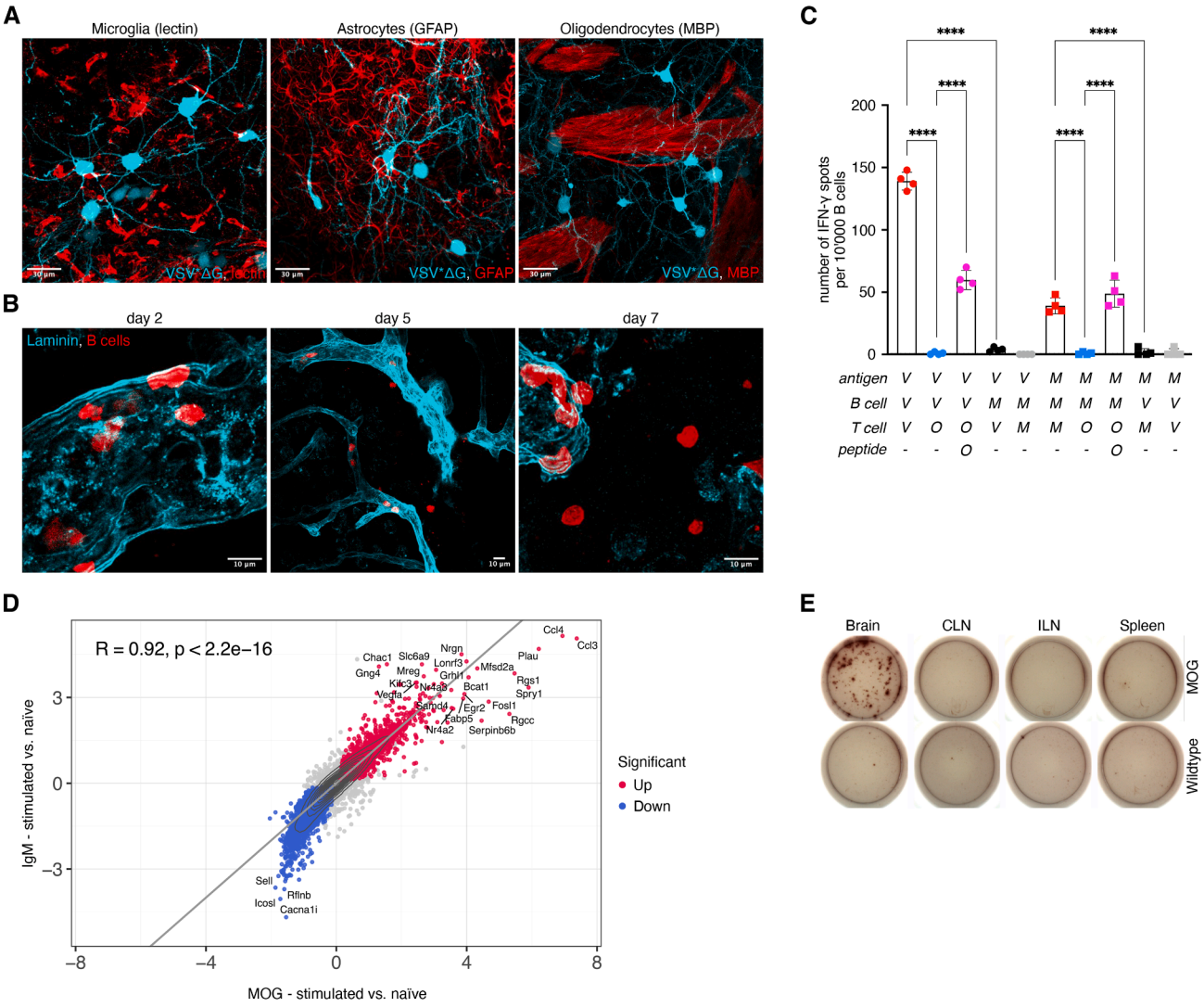

Figure S2. B cell CNS infiltration following infection, related to Figure 2

(A) Cellular tropism of VSV*ΔG in brain. Confocal micrographs of sections of infected brain, each labeled for a different cell type marker (red) together with VSV-encoded GFP (cyan). From left to right, the three images show microglia labeled with *Lycopersicon esculentum* lectin, astrocytes immunolabeled for GFAP, and oligodendrocytes labeled for MBP. Scale bars, 30 μm.

(B) Perivascular-to-parenchymal infiltration of B cells over 2–7 days. B cells express tdTomato (red) and laminin labeling of the vascular basement membrane is shown in cyan. Scale bars, 10 μm.

(C) Sensitivity and specificity of the ELISpot technique. MOG ("M") or V10 B cells ("V") from the spleens of naive animals, exposed or not to the cognate or mismatched antigen ("V": TE 617 cells expressing VSV glycoprotein; "M": TE 671 cells expressing MOG), and additionally pulsed or not with chicken ovalbumin peptide ("O"). Cells were then cultured in ELISpot plates with 2D2("M"), L7 ("V"), or OT-II ("O") T cells, and interferon-γ spots were visualized and counted 5 days later. ****$p < 0.0001$, one-way ANOVA followed by SIDAK'S multiple-comparisons test.

(D) Comparison of gene transcription between MOG tomato B cells exposed to MOG-expressing target cells for 4 h and similar B cells stimulated with anti-IgM antibody for the same duration. Genes with a $\log_2$ fold difference higher than 3.5 are labeled with their symbols.

(E) Representative ELISpot wells from B cell MOG capture assay. The upper row are images from wells containing B cells from MOG tomato mice, and the lower row from WT tomato mice. B cells were taken from the four different anatomical sources, as specified above the images.

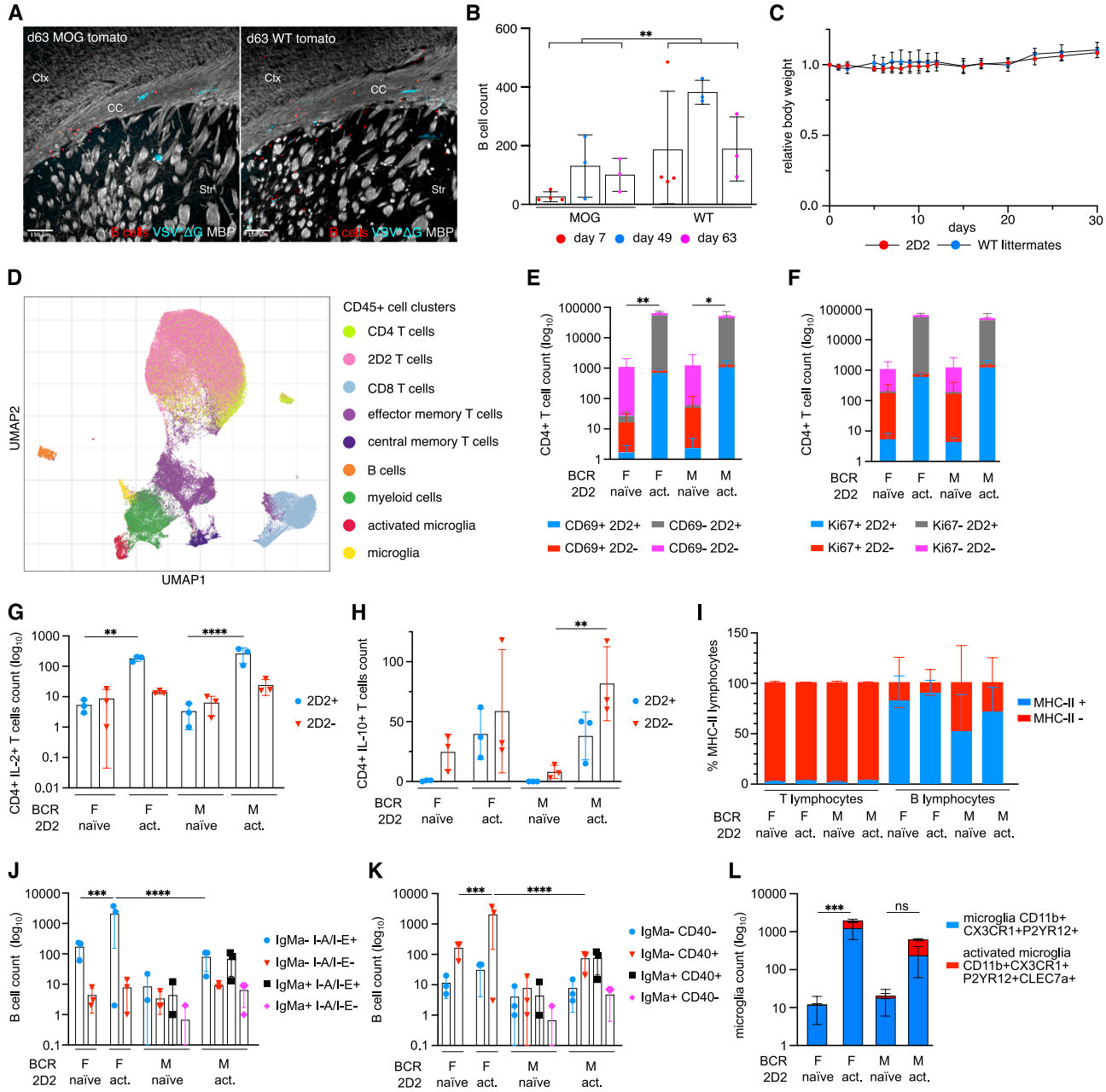

Figure S3. CNS lymphocyte infiltration, related to Figure 3

(A) Fluorescent micrographs of coronal sections through MOG tomato (left image) or WT tomato (right image) mice sacrificed 63 days after intrastriatal infection with VSV*ΔG. White: MBP immunolabeling; red: tdTomato (B cells); cyan: GFP (VSV*DG). Ctx, cerebral cortex; CC, corpus callosum; str, striatum. Scale bar, 150 μm.

(B) Numbers of brain-infiltrating B cells in MOG tomato (left three bars) and WT tomato (right three bars) mice at various time points after intrastriatal infection with VSV*DG. $^{**}p = 0.0053$, two-way ANOVA, main effect of genotype.

(C) Weights of 2D2 (red circles) or WT littermate (blue circles) mice infected in the striatum with VSV*DG and transferred with MOG tomato B cells, over 28 days following infection.

(D–K) Influence on brain-infiltrating immune cell phenotype of activated T cells, in the presence of cognate B cells. Four experimental conditions were analyzed. MOG (M) or FluBl (F) mice were infected intrastriatally with VSV*DG and adoptively transferred with naive (naive) or activated (act.) 2D2 T cells, then sacrificed 12 days later for flow cytometry of brain-infiltrating immune cells. (D) Omnibus UMAP plot, analogous to Figure 3M, of immune cells infiltrating the brain in all four conditions pooled. (E) Numbers of $CD69^+$ and $CD69-$ $CD4^+$ T cells in the four groups, split by 2D2 transgenic or non-transgenic TCR. *p* values correspond to all $CD4^+$ T cells (i.e., the total height of each bar) $^{*}p = 0.0270$, $^{**}p = 0.0088$, two-way ANOVA. (F) Numbers of Ki67+ and Ki67− $CD4^+$ T cells in the four groups, split by 2D2 transgenic or non-transgenic TCR. *p* values identical to (E). (G) Numbers of IL-2+ and IL-2− $CD4^+$ T cells in the four groups, split by 2D2 transgenic or non-

(legend continued on next page)

transgenic TCR. $^{**}p = 0.0031$, $^{****}p < 0.0001$, two-way ANOVA. (H) Numbers of IL-10+ and IL-10− $CD4^+$ T cells in the four groups, split by 2D2 transgenic or non-transgenic TCR. $^{**}p = 0.009$, two-way ANOVA. (I) Percentages of MHC class II-expressing (blue sub-bars) and non-expressing (red sub-bars) cells in the four groups. The left four bars show T cells, and the right four bars show B cells. (J) Numbers of MHC class II-expressing and non-expressing MOG transgenic (IgMa+) and non-transgenic (IgMa−) B cells in the four groups. $^{***}p = 0.0002$, $^{****}p < 0.0001$, two-way ANOVA. (K) Numbers of CD40- expressing and non-expressing MOG transgenic (IgMa+) and non-transgenic (IgMa−) B cells in the four groups. $^{***}p = 0.0002$, $^{****}p < 0.0001$, two-way ANOVA.
(L) Numbers of microglia expressing or not expressing the activation marker Clec7a. $^{***}p = 0.0002$.

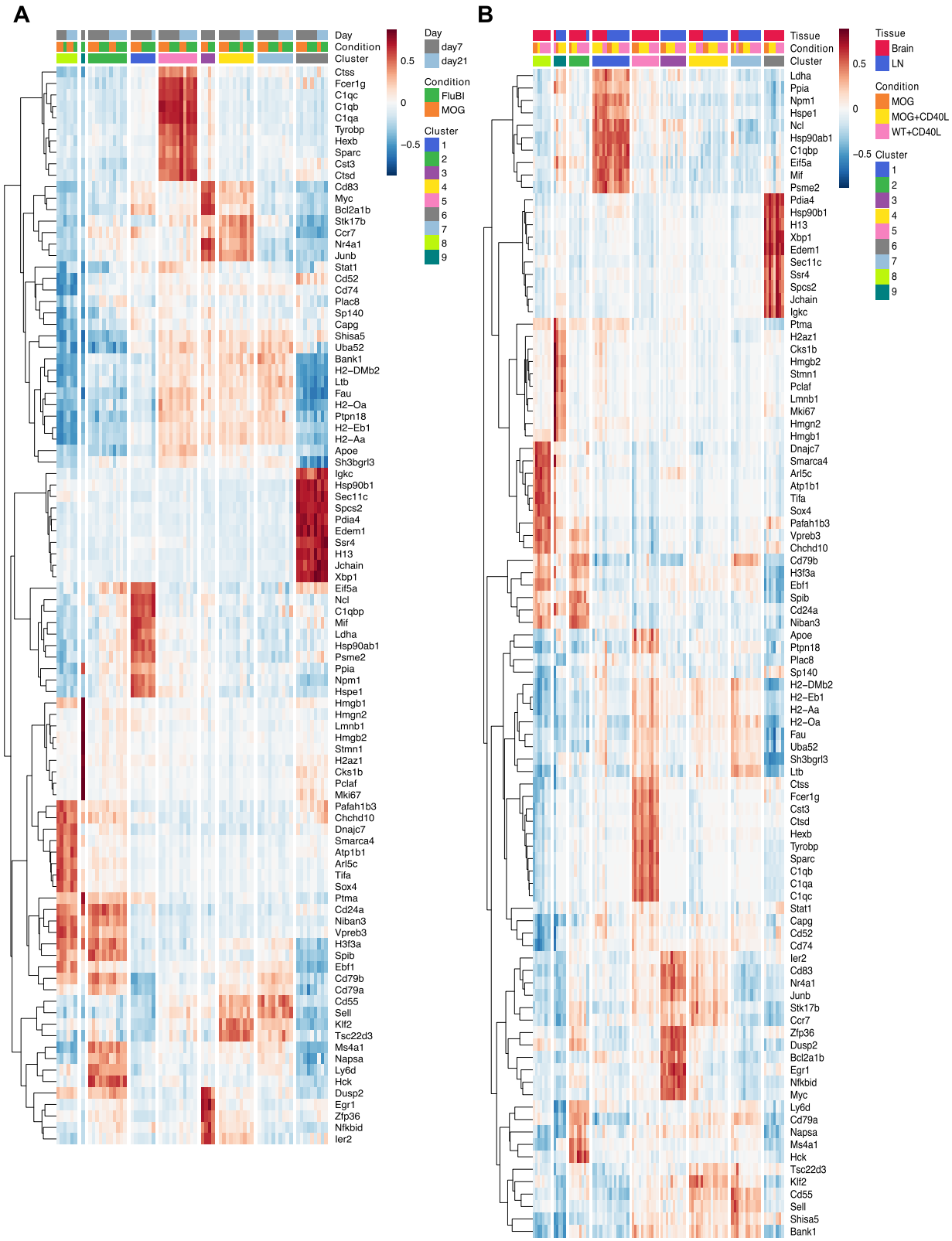

(legend on next page)

Figure S4. Gene expression heatmaps defining clusters, related to Figures 3 and 4

Heatmap on the left shows expression of genes defining the nine clusters shown in Figure 3B and heatmap on the right shows expression of genes defining the 11 clusters shown in Figure 4F.

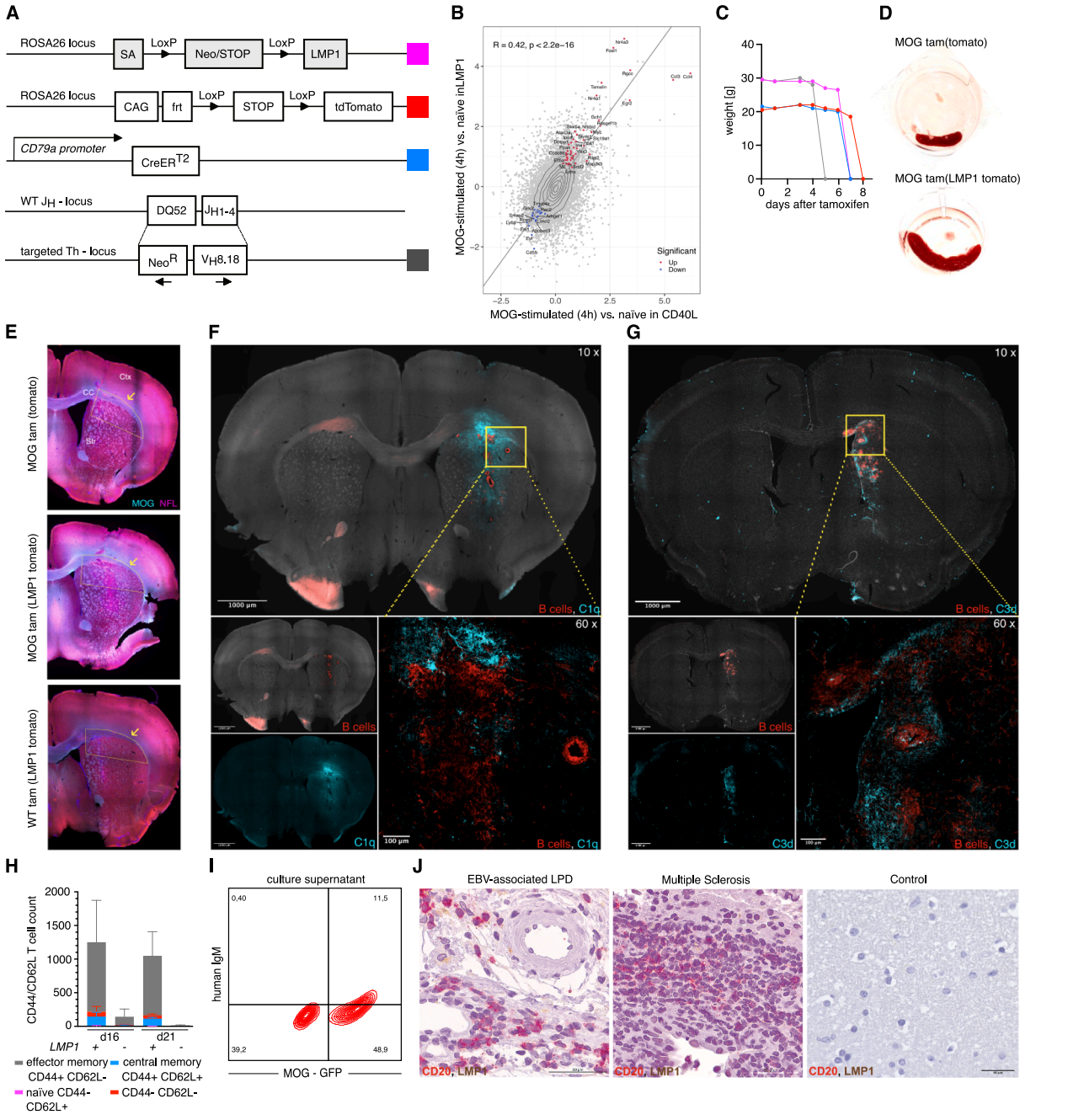

(legend on next page)

Figure S5. Inducible LMP1 expression in B cells, related to Figures 5 and 6

(A) More detailed depiction of the alleles involved in the schematic breeding scheme shown in Figure 5A.

(B) Comparison of transcription changes in response to antigen encounter by B cells expressing LMP1 or exposed to CD40L. Genes significantly upregulated in both conditions are plotted with red points, and those downregulated in both conditions are plotted in blue.

(C) Weights of MOG tam(LMP1 tomato) mice in which global, B cell-restricted LMP1 expression was induced by systemic tamoxifen administration. Animals were euthanized at pre-specified humane endpoints defined by weight loss.

(D) Spleens taken from MOG tam(tomato) (left) or MOG tam(LMP1 tomato) mice given systemic tamoxifen and euthanized 4 days later.

(E) Fluorescent micrographs of coronal sections through mouse brains showing standardized regions of interest (yellow outlines) from which areas of demyelination were extracted by an automated algorithm for the analysis of images shown in Figures 6H and 6I. Ctx, cerebral cortex; CC, corpus callosum; Str, striatum. Myelin (MOG) immunolabeling is shown in blue, and axons (neurofilament, NFL) in magenta.

(F) Fluorescent micrographs of coronal sections through mouse brain showing C1q immunolabeling (cyan) in the vicinity of the B cell-induced lesion. Scale bar, 1 mm. The lower right image is a higher-powered confocal micrograph of the area highlighted in yellow. Scale bar, 100 μm.

(G) Fluorescent micrographs of coronal sections through mouse brain showing C3d immunolabeling (cyan) in the vicinity of the B cell-induced lesion. Scale bar, 1 mm. The lower right image is a higher-powered confocal micrograph of the area highlighted in yellow. Scale bar, 100 μm.

(H) Phenotypes of brain-infiltrating T cells at two time points in mice with endogenous 2D2 T cells and transferred with tamoxifen-induced MOG tam(LMP1 tomato) or MOG tam(tomato) B cells

(I) Antigen specificity of an antibody secreted by a single B cell from a healthy human. Antibody-containing culture supernatant was incubated with a mixture of MOG-expressing and non-expressing cells. Bound antibody was detected with class-specific fluorescent anti-human secondary antibodies and measured by flow cytometry. The vertical axis shows antibody signal, and the horizontal axis shows GFP used to distinguish the MOG antigen-expressing cells.

(J) Two-color immunohistochemistry of LMP1 (brown) and CD20 (red) in human biopsy tissue. Left panel shows sample from a patient with an EBV-associated lymphoproliferative disorder without detectable LMP1 signal. Center panel comes from a patient with MS, with numerous $CD20^{+}$ B cells, also negative for LMP1. Right panel shows an example of the same immunolabeling of brain tissue from a control donor with no neurological disease and no CD20 or LMP1 signal detectable. Scale bar, 50 μm.

(K) Two-color immunofluorescence of LMP1 (cyan) and CD20 (red) in human biopsy tissue. The left-most panel shows tissue from EBV-positive lymphoma and contains numerous double-positive cells. The middle panel shows tissue from MS lesion and contains a small number of double-positive cells; a larger field of view is included to show the structure of a perivascular cuff of immune cells. The right-most image is from another MS lesion showing numerous CD20-positive B cells but no LMP1 signal. Smaller images in each panel show single channels. Scale bars, 10 and 20 μm, as shown.